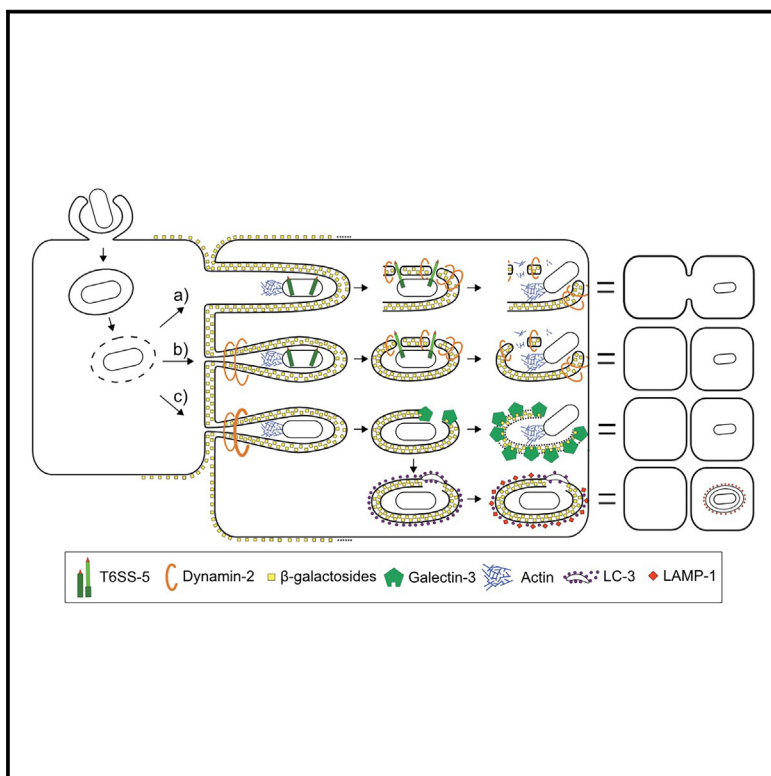


Cell Host & Microbe

***Burkholderia thailandensis* uses a type VI secretion system to lyse protrusions without triggering host cell responses**

Graphical abstract



Authors

Miro Thorsten Wilhelm Plum,
Hoi Ching Cheung, Patricia Reist Iscar,
Yahua Chen, Yunn-Hwen Gan,
Marek Basler

Correspondence

marek.basler@unibas.ch

In brief

Plum et al. uncover a stealthy mechanism by which the intracellular pathogen *Burkholderia thailandensis* spreads between host cells. The bacteria form membrane protrusions and lyse them using the type VI secretion system, which prevents recognition by host cell defense mechanisms. This expands our understanding of bacterial behavior and host-pathogen interactions.

Highlights

- *B. thailandensis* spreads from cell to cell by forming and lysing membrane protrusions
- The bacteria specifically activate the assembly of their T6SS-5 in the protrusions
- Efficient protrusion lysis and bacterial spread depend on T6SS-5 and host dynamin
- T6SS-5 activity decreases recruitment of Gal-3, LC3, and LAMP1 to bacteria



Article

Burkholderia thailandensis uses a type VI secretion system to lyse protrusions without triggering host cell responses

Miro Thorsten Wilhelm Plum,¹ Hoi Ching Cheung,¹ Patricia Reist Iscar,¹ Yahua Chen,² Yunn-Hwen Gan,² and Marek Basler^{1,3,*}

¹Biozentrum, University of Basel, Spitalstrasse 41, 4056 Basel, Switzerland

²Department of Biochemistry, National University of Singapore, 8 Medical Drive, Singapore 117596, Singapore

³Lead contact

*Correspondence: marek.basler@unibas.ch

<https://doi.org/10.1016/j.chom.2024.03.013>

SUMMARY

To spread within a host, intracellular *Burkholderia* form actin tails to generate membrane protrusions into neighboring host cells and use type VI secretion system-5 (T6SS-5) to induce cell-cell fusions. Here, we show that *B. thailandensis* also uses T6SS-5 to lyse protrusions to directly spread from cell to cell. Dynamin-2 recruitment to the membrane near a bacterium was followed by a short burst of T6SS-5 activity. This resulted in the polymerization of the actin of the newly invaded host cell and disruption of the protrusion membrane. Most protrusion lysis events were dependent on dynamin activity, caused no cell-cell fusion, and failed to be recognized by galectin-3. T6SS-5 inactivation decreased protrusion lysis but increased galectin-3, LC3, and LAMP1 accumulation in host cells. Our results indicate that *B. thailandensis* specifically activates T6SS-5 assembly in membrane protrusions to disrupt host cell membranes and spread without alerting cellular responses, such as autophagy.

INTRODUCTION

Intracellular pathogens avoid and manipulate eukaryotic host responses to better survive in their niche. The facultative intracellular bacterial pathogen *Burkholderia pseudomallei* is endemic in tropical and subtropical regions and causes an estimated 165,000 cases per year of the disease melioidosis of which 89,000 are estimated to be fatal.^{1–3} Patients with melioidosis are commonly infected from the environment via inhalation, ingestion, or skin abrasions.^{4,5} Due to the high mortality rate of melioidosis and the pathogen's intrinsic high resistance to antibiotics, *B. pseudomallei* is considered a tier 1 select agent by the US Centers for Disease Control and Prevention.⁶ The closely related species *B. thailandensis* is commonly used as an attenuated model for *B. pseudomallei* because it is less virulent for humans, but it is still able to cause disease in mice and other model organisms.^{7,8}

Both *B. pseudomallei* and *B. thailandensis* are able to infect a wide variety of eukaryotic host cells.⁹ After uptake into the primary vacuole, which can be either the phagosome or the endosome, *B. thailandensis* escapes from it by secreting a cocktail of effectors with its type III secretion system (T3SS).^{10,11} Once inside the host cell cytoplasm, *B. thailandensis* uses either BimA to induce the formation of actin tails and/or flagella to move around inside the host cell.^{11,12} BimA of *B. thailandensis* activates the host's Arp 2/3 complex to form actin tails, whereas

B. pseudomallei mimics Ena/VASP actin polymerase.¹² In addition, actin tails allow *B. thailandensis* to form long membranous protrusions from one host cell into a neighboring host cell, similar to other intracellular pathogens, such as *Shigella flexneri*.^{13,14} For other intracellular pathogens, the resolution of these membranous protrusions was shown to be dependent on clathrin-mediated endocytic host pathways that involved dynamin-2.^{15,16} Furthermore, *B. thailandensis* fuses two or more host cells, leading to the formation of multi-nucleated giant cells (MNGCs).¹³ MNGCs formation was shown to be dependent on intracellular motility and a type VI secretion system (T6SS).^{11,17} However, INF- γ -activated human epithelial cells were shown to restrict MNGC formation by inducing GBP-1- and caspase-4-dependent pyroptotic cell death.¹⁸

T6SS is a contractile injection system^{19–22} composed of a membrane complex (TssM/L/J) connected to a baseplate (TssE/F/G/K) with VgrG/PAAR spike protein in the center.^{23–25} TssB/TssC forms a long contractile polymer called a sheath around the inner tube composed of Hcp.^{23,26,27} Sheath contraction pushes the spike and tube with associated effectors into a neighboring bacterial or eukaryotic cell.^{19,28–31} The AAA(+) ATPase ClpV disassembles the contracted sheath to allow new round of T6SS assembly.^{32–34} T6SS activity is commonly visualized by a fluorescent protein fusion to either TssB or ClpV.^{32,34} In *B. thailandensis*, it was shown that the C-terminal domain (CTD) of VgrG-5, containing three predicted



transmembrane helices, is required for the formation of MNGCs.^{17,35} However, it is unknown whether VgrG-5 alone is sufficient to cause MNGC formation or if there are other effectors involved. Genes encoding T6SS effectors are usually located downstream of their respective VgrGs.^{36–39} Interestingly, the T6SS-5 cluster has four genes *tagC-5*, *tagB-5*, *tagAB-5*, and *tagD-5* downstream of *vgrG-5*, although their exact function remains unknown.^{40–42} Only TagD-5 was shown to be involved in the cell-cell fusion step during MNGC formation, and TagAB-5 was shown to affect Hcp-5 secretion in *B. pseudomallei*.^{40,42}

To understand how T6SS-5 assembly leads to MNGC formation or membrane protrusion lysis, we visualized *B. thailandensis* T6SS-5 dynamics during infection of HeLa and A549 lung cells, both known to allow T6SS-5 expression and form MNGCs.^{13,43,44} We observed that *B. thailandensis* moves from cell to cell by forming membrane protrusions where most T6SS-5 assembles and contributes to their lysis. Dynamin-2 localization to membranes around the bacteria was observed shortly before and after T6SS-5 activity, and cell-autonomous immunity systems failed to detect T6SS-5-dependent protrusion lysis, suggesting that *B. thailandensis* uses a unique mechanism to spread from cell to cell without alarming the host.

RESULTS

T6SS-5 assembly localizes preferentially to bacterial poles and is dependent on accessory genes

To analyze T6SS-5 activity during infection, we fused the TssB-5 C terminus with mCherry2, mScarlet-I, msfGFP, or mNeon-Green. Because MNGC formation is a hallmark of a functional T6SS-5,^{11,45,46} we tested if TssB-5 fluorescent protein fusions impact the formation of MNGCs. We infected a mixture of HeLa cells expressing either a red (galectin-3-mApple) or a green (galectin-3-GFP) cytosolic fluorescent protein and analyzed the formation of cells with both fluorescently labeled proteins. We used this cell line because it was previously shown that *Burkholderia* forms MNGCs in HeLa cells, and this cell line was available with the appropriate markers to readily detect MNGC formation.^{13,43,44} The cells were seeded to confluence and infected at a multiplicity of infection (MOI) of 50 for 1 h. Extracellular bacteria were then removed with several washes, and kanamycin was added into the medium to kill extracellular bacteria. Upon 12 h of incubation, MNGCs were detected for the *B. thailandensis* parental strain, as well as the strains expressing TssB-5 fusion proteins (Figures 1A and S1A). To quantify MNGC formation, we infected A549 lung cells at a MOI of 50 for 1 h. At 15–16 h post infection (hpi), the cells were fixed with 100% methanol and visualized with Giemsa stain. We analyzed 12 fields of view (500 μm × 500 μm) in two biological replicates and showed that most strains induced comparable levels of MNGC formation, with the exception of the TssB-5-mNeonGreen and TssB-5-msfGFP strains (Figures S1B and S1C). No MNGC formation was observed for the T6SS-5-negative strains (deletion of *hcp-5* or *vgrG-5*). Next, we tested the size of plaques forming upon cell-cell fusions.^{11,12} For this, we seeded 6-well plates with A549 lung cells and infected them at an MOI of 2. A549 cells are commonly used for plaque assays, and *B. thailandensis* infects lung epithelial cells during infection.^{4,12,47} The cells were imaged at 31 hpi, and the average plaque size was calcu-

lated from at least 11 plaques in 3 biological replicates. A significant reduction in plaque size was detected for the TssB-5-mNeonGreen strain, and no plaques were formed by the T6SS-5-negative strains (Figures S1D and S1E).

To analyze the dynamics of T6SS-5 during infection, HeLa cells were infected at an MOI of 50 for 1 h, and TssB-5 localization was followed using fluorescence microscopy. A dynamic localization pattern consistent with sheath assembly, contraction, and disassembly was observed for all TssB-5 sheath-fluorescent protein fusions (Figures 1B, 1C, and S1F; Video S1). We analyzed 426 cells of the TssB-5-mScarlet-I strain and detected at least one T6SS-5 assembly in 103 (24.3%) bacteria during the 1-h imaging period. We imaged 30 assembly events at a frame rate of 4 or 10 s per frame to show that T6SS-5 assembly takes from 30 to 80 s, with an average of 48 s (Video S1). In addition, out of 173 TssB-5-mScarlet-I sheath assemblies, 129 (75%) assemblies originated from the bacterial poles compared with 44 (25%) assemblies that were non-polar localized. This is consistent with the previous observation that 77% of ClpV-5-sfGFP spots were polarly localized.¹⁷

To test if the observed T6SS-5 sheath dynamics and localization depend on genes encoded in the T6SS-5 cluster, we introduced TssB-5-mCherry2 or TssB-5-mNeonGreen into *hcp-5*, *vgrG5*, *tagAB-5*, *tagB-5*, *tagC-5*, and *tagD-5* deletion strains (*hcp-5* and *vgrG-5* deletion strains provided by the Gan lab) (Figure S1G). We analyzed sheath assembly in at least 216 bacteria in 4 fields of view (250 μm × 250 μm) for each strain at 12–17 hpi during a 10-min imaging period. Although TssB-5-mCherry2 or TssB-5-mNeonGreen was expressed to comparable levels in all tested strains, we detected no sheath assemblies in any of the tested deletion strains (Figure S1H). Overall, we show that TssB-5 fusion to most fluorescent proteins has little to no impact on the ability of *B. thailandensis* to induce MNGC and that T6SS-5 is highly dynamic, preferentially assembles at the bacterial pole, and its assembly depends on *hcp-5*, *vgrG-5*, and the accessory genes *tagAB-5*, *tagB-5*, *tagC-5*, and *tagD-5*.

B. thailandensis spreads from cell to cell beyond MNGC formation

B. thailandensis was shown to spread from cell to cell via the formation of MNGCs.^{11,45,46} To investigate the progression of MNGC formation in time, we infected A549 cells with the *B. thailandensis* parental strain at an MOI of 10 to initiate infections from individual cells that are surrounded by uninfected cells. A549 cells infected by *B. thailandensis* form MNGCs comparable to natural infections.^{4,13,43,44} We used the lipophilic CellMask DeepRed Plasma membrane dye (CM) to stain host cell membranes and Hoechst 33342 to stain nuclei to visualize the formation of MNGCs from 5:30 to 20:00 hpi. Importantly, the medium contained kanamycin to kill extracellular bacteria to prevent infection by bacteria escaping over time from infected host cells. We have defined an MNGC as a cell with at least two nuclei present throughout the time-lapse (to avoid counting dividing cells) and containing bacteria within its cytoplasm. Time-lapse imaging revealed that the first MNGCs were formed at 5:30 hpi and progressively increased in size (Figure 1D; Video S2). Over time, small MNGCs fused into one large MNGC that eventually lysed. Interestingly, we observed bacteria several host cells away from the closest MNGC (Figure 1D). No MNGC

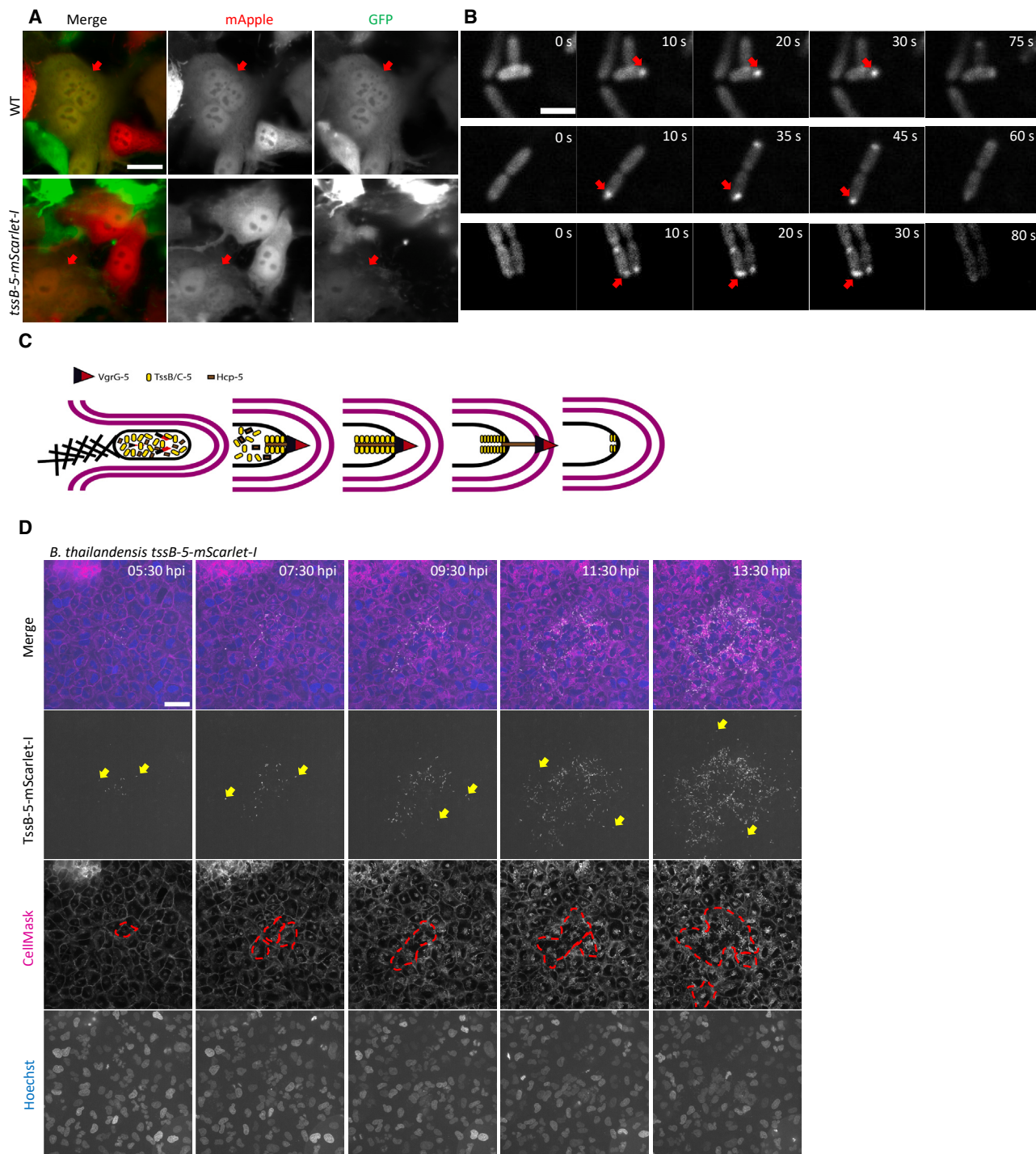


Figure 1. *TssB-5-mScarlet-I* expressing bacteria assembles functional T6SS-5 and spreads beyond MNGC

(A) HeLa-CCL2 cells expressing either galectin-3-GFP or galectin-3-mApple (mixed 1:1) were infected with *B. thailandensis* wild type (WT) or *B. thailandensis* *TssB-5-mScarlet-I* (MOI 50). Cells were imaged at 17–18 hpi to detect the presence of cells containing both galectin-3-GFP and galectin-3-mApple, indicating MNGC formation. The left image shows a merge of the mApple and GFP channels shown individually in grayscale on the right. Scale bar represents 20 μ m.

(B) HeLa-CCL2 cells infected with *B. thailandensis* *TssB-5-mScarlet-I* (MOI 50). T6SS-5 assemblies imaged at 18 hpi, framerate of 5–10 s. Red arrows indicate T6SS-5 assembly. Scale bar represents 2 μ m. Time-lapse in [Video S1](#).

(C) Schematic of T6SS-5 dynamics inside of membrane protrusions.

(D) A549 lung cells infected with *B. thailandensis* *TssB-5-mScarlet-I* (gray scale) (MOI 10). Host membranes stained with CellMask DeepRed (magenta), nuclei with Hoechst 33342 (blue). Images were acquired from 5:30 to 20:00 hpi every 10 min (295 μ m \times 295 μ m field of view). MNGCs are marked with a dotted red line, and bacteria outside of MNGCs are marked with yellow arrows. The scale bar represents 50 μ m. Time-lapse in [Video S2](#).

See also [Figures S1](#) and [S2](#).

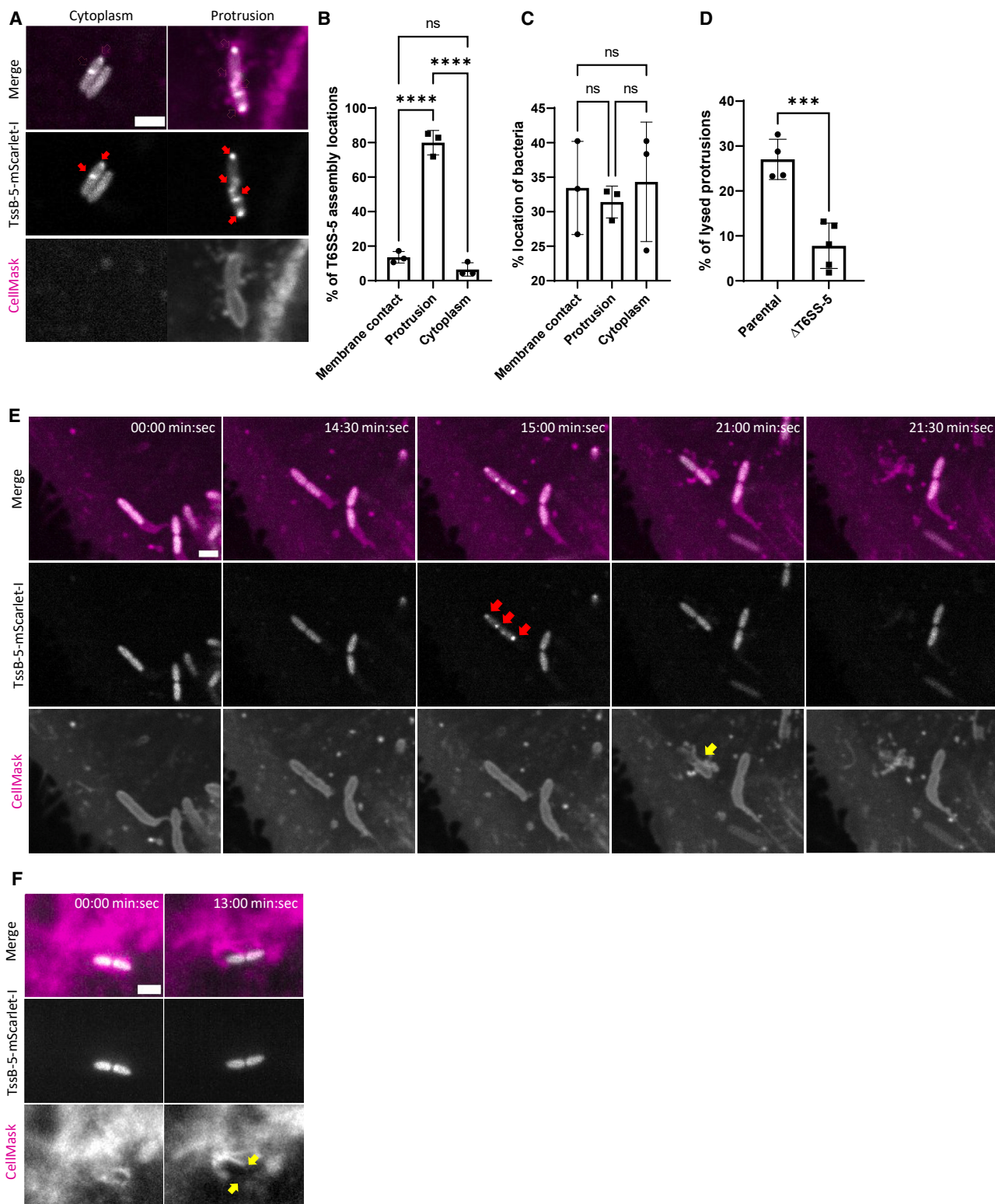


Figure 2. *B. thailandensis* T6SS-5 assembles mostly in protrusions and causes their lysis

(A) T6SS-5 assemblies in bacteria in the host cytoplasm or with contact to the host membrane. HeLa-CCL2 cells were infected with *B. thailandensis* at an MOI 50 (stained with CellMask DeepRed). The top images show the merge of T6SS-5 (TssB-5-mScarlet-I, grayscale) and host cell membranes (CellMask DeepRed, magenta). The left image: cytosolic *B. thailandensis* with T6SS-5 sheaths. The right image: *B. thailandensis* in a membrane protrusion with T6SS-5 sheaths. Images below show individual channels in gray scale. Images were taken at 14 hpi. Red arrows indicate T6SS-5 assemblies. Scale bar represents 2 μm.

(legend continued on next page)

formation was observed for the $\Delta hcp-5$ strain; however, the mutant was still able to spread from cell to cell, albeit at a reduced rate compared with the parental strain (Figure S2; Video S2). This indicates that *B. thailandensis* can spread from cell to cell without MNGC formation and that the rate of this direct cell-to-cell spread is increased by T6SS-5.

***B. thailandensis* T6SS-5 preferentially assembles in host cell protrusions**

B. thailandensis was shown to form actin tails and cell membrane protrusions while requiring T6SS-5 and its components VgrG-5 and TagD-5 to lyse protrusions to form MNGCs.^{12,17,35,42} Because we observed a T6SS-5-dependent increase in direct cell-to-cell spread in addition to MNGC formation, we set out to correlate T6SS-5 assembly with the lysis of protrusions. We infected HeLa cells with *B. thailandensis* expressing TssB-5-mScarlet-I at an MOI of 50 as described above. We imaged localization of TssB-5 and host membranes (labeled with CM) with a framerate of 30 s per frame over a 1-h period at 11–16 hpi. We detected 763 bacteria in 9 fields of view (81 $\mu\text{m} \times 81 \mu\text{m}$) in three biological replicates, and 17% showed at least one T6SS-5 assembly (sheath assembly, contraction, and disassembly) during a 1-h imaging period. The location of 130 bacteria with at least one T6SS-5 assembly was classified as either cytoplasmic or in contact or surrounded by host cell membranes (protrusions) (Figure 2A). Interestingly, in these bacteria, we detected 228 T6SS-5 assemblies, and only 14 assemblies took place in bacteria residing in the cytoplasm, whereas 214 assemblies were detected in bacteria that were in contact with the host membrane (31 assemblies, 14%) or in the host cell membrane protrusions (183 assemblies, 80%) (Figure 2B). A general distribution of bacteria within the host cells was estimated by the analysis of the first frame of the time-lapses. Out of the 255 identified bacteria, 34% were in contact with membranes, 31% in protrusions, and 35% in the cytoplasm (Figure 2C). Together, this indicates that T6SS-5 assembly is specifically activated when *B. thailandensis* are in protrusions.

T6SS-5 contributes to lysis of membrane protrusions, but only a subset of lysis events lead to MNGC formation

To test whether T6SS-5 activity correlates with the lysis of membranes and how often those lead to cell-cell fusion, we analyzed the rate of protrusion formation and lysis, as well as MNGC formation, during a 1-h imaging period. We mixed two HeLa cell lines (one expressing the cytoplasmic protein galectin-3-GFP

and one without a marker), stained them with CM, and infected them at an MOI of 50 with the *B. thailandensis* TssB-5-mScarlet-I strain. We define here the protrusion lysis event as the moment when we detected membrane rupture and fragmentation around the bacterium. Only protrusions that were visible during 1 h or till their lysis were counted. Cell-cell fusions were identified by detecting the relocalization of the GFP signal to an unlabeled cell or by detecting membrane rupture. Due to the limited number of in-focus protrusion lysis events leading to MNGC formation, as well as challenges in identifying the exact bacterium responsible for causing cell-cell fusion, we counted protrusion lysis and MNGC formation independently from one another. In three biological replicates, we analyzed 22 and 35 fields of view (81 $\mu\text{m} \times 81 \mu\text{m}$) for the T6SS-5-positive or -negative strains, respectively. For the T6SS-5 positive strain, we identified 337 protrusions, of which 91 (27%) lysed (Figures 2D, 2E, and S3; Video S3). Moreover, the T6SS-5 assembly event was detected within 90 s of 72 (79%) of the membrane protrusion lysis events. In contrast, for T6SS-5-negative strains (*hcp-5* or *vgrG-5* negative), only 23 of 289 (8%) protrusions lysed (Figures 2D and 2F; t test, $p = 0.0006$). This suggests that the T6SS-5 activity increases the likelihood of bacterial escape from protrusions by over 3-fold and thus plays a significant role in promoting protrusion lysis. Interestingly, for those 91 protrusion lysis events (detected in 22 fields of view), we observed only 16 subsequent MNGC formations in the same fields of view (Figures 3A, 3B, S4A, and S4B; Video S4). The data suggest that only around 1 in 6 protrusion lysis events lead to the formation of MNGCs and that protrusion lysis is the predominant mechanism of intercellular spread of *B. thailandensis* in this model.

Dynamin is important for protrusion lysis

Dynamin-2 was shown to be important for the membrane protrusion-based cell-to-cell spread of *S. flexneri*.^{16,48} To test the role of dynamin during *B. thailandensis* host cell infection, we used the GTPase inhibitor dynasore to evaluate its influence on protrusion lysis and MNGC formation.^{48,49} Infections of A549 cells were performed as described above, and 120 μM dynasore or DMSO was added 1 h before imaging. A total of 6 fields of view (295 $\mu\text{m} \times 295 \mu\text{m}$) were imaged for two biological replicates at 13:30–15:30 hpi. Interestingly, protrusions that formed in the dynasore-treated cells appeared longer and showed delayed lysis or remained intact during the 1-h imaging period (Figures 4A and S5A). We analyzed the formation and lysis of

(B) Quantification of T6SS-5 assembling bacteria classified as: in contact with host membranes, surrounded by host membranes (protrusions), or in the cytoplasm without membrane contact. 298 T6SS-5 assemblies, three biological replicates. One-way ANOVA used to determine the statistical significance (ns: not significant, *** $p < 0.001$).

(C) 255 bacteria were counted in 9 images (81 $\mu\text{m} \times 81 \mu\text{m}$) in three biological replicates, with location classified as in (B). One-way ANOVA used to determine the statistical significance (ns: not significant).

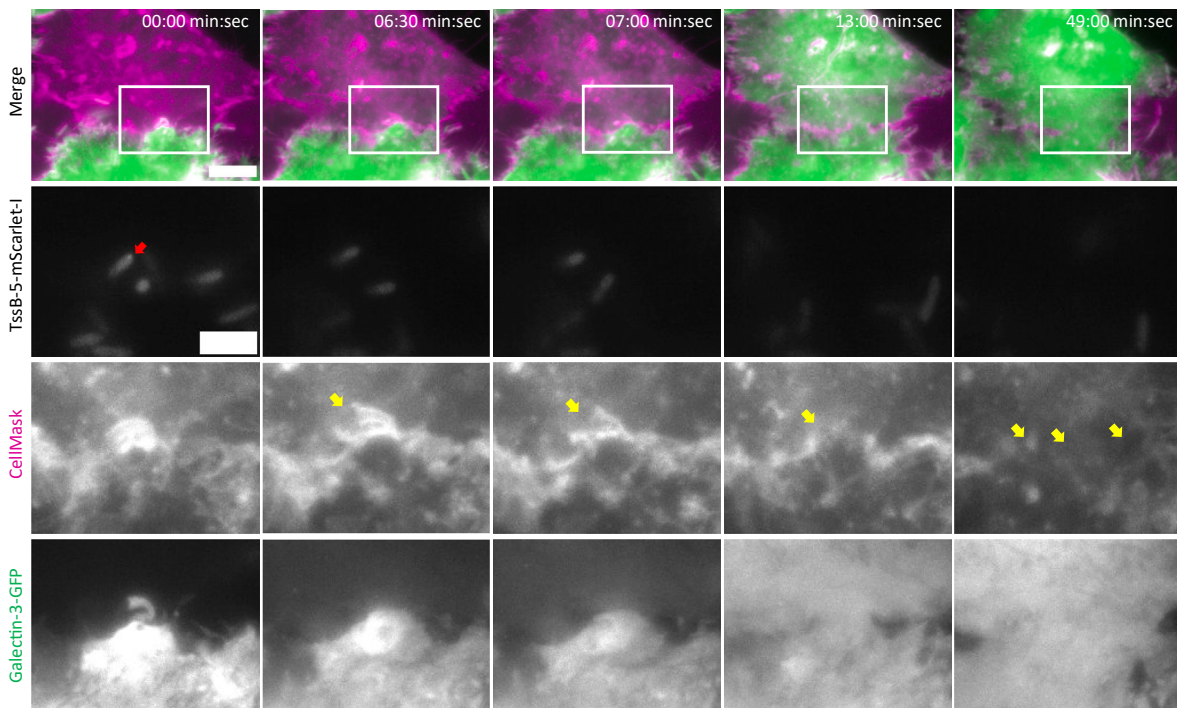
(D) Percentage of protrusions lysed during a 1-h imaging period by the parental TssB-5-mScarlet-I and the Δ T6SS-5 ($\Delta hcp-5$ or $\Delta vgrG-5$) *B. thailandensis* strains. For the parental strain, 337 protrusions were counted in 22 fields of view (81 $\mu\text{m} \times 81 \mu\text{m}$). For the Δ T6SS-5 strains, 289 protrusions were counted in 35 fields of view (81 $\mu\text{m} \times 81 \mu\text{m}$). Images taken at 11–17 hpi. Data was compiled from three independent experiments. A two-tailed unpaired t test was performed (** $p < 0.001$).

(E) T6SS-5-dependent protrusion lysis. A549 cells were infected with *B. thailandensis* TssB-5-mScarlet-I. Red arrows indicate T6SS-5 assemblies. Lysis of protrusions indicated by a yellow arrow. Time-lapse in Video S3. The images taken from 13:45 hpi. Scale bar represents 2 μm .

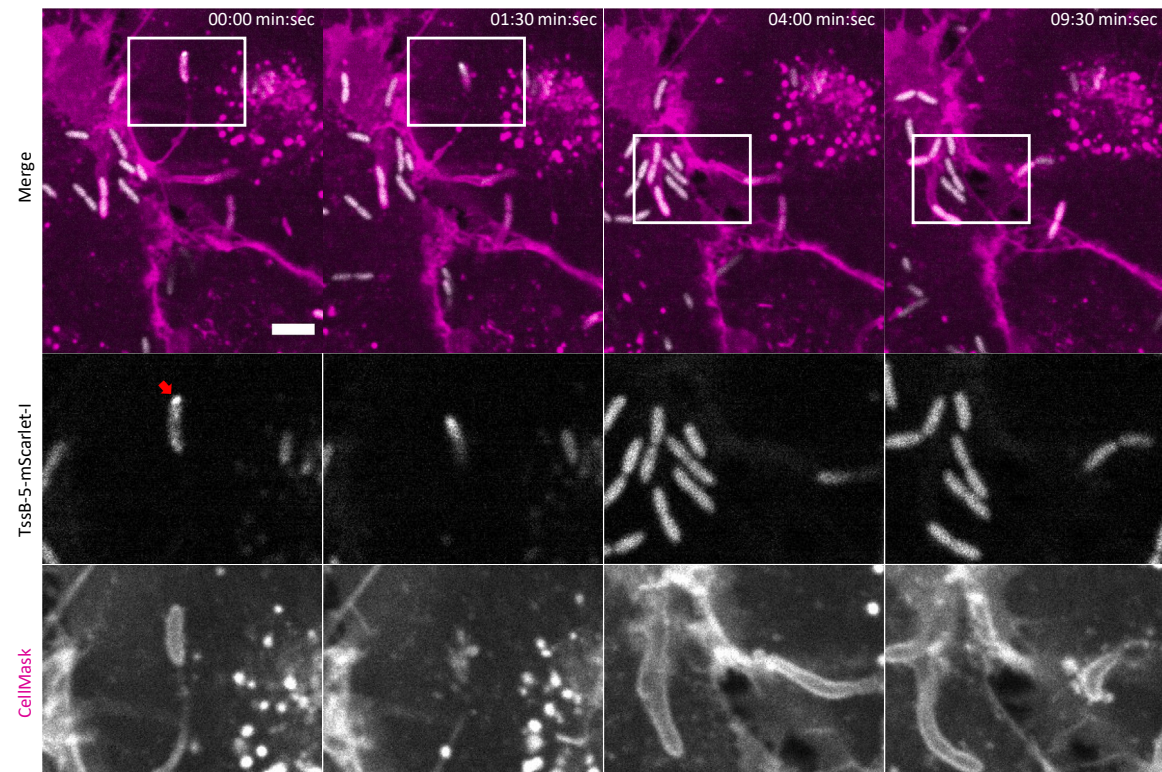
(F) T6SS-5-independent protrusion lysis. A549 cells were infected with *B. thailandensis* TssB-5-mScarlet-I $\Delta hcp-5$. Lysis of protrusions are indicated by a yellow arrow. Images acquired at 11 hpi. Scale bar represents 2 μm .

See also Figure S3.

A



B



(legend on next page)

523 protrusions in dynasore-treated and 508 protrusions in DMSO-treated cells during a 1-h time period (Figure 4B). Dynasore-treated cells showed a marked decrease in protrusion lysis, with only 50 (10%) protrusion lysis events compared with 126 (25%) in the DMSO-treated control (*t* test, $p = 0.0006$). To investigate if dynasore treatment influences MNGC formation, we infected A549 cells as described above and added 120 μ M dynasore or DMSO at 1 hpi. Cells were fixed at 14 or 16 hpi and Giemsa stained to analyze MNGC formation (over 2,000 nuclei counted per biological replicate). Interestingly both the dynasore-treated and the DMSO control showed comparable levels of MNGC formations (Figures 4C and 4D).

Dynasore was shown to have off-target effects, including inhibition of other host cell GTPases and effects on cellular cholesterol.^{49,50} Therefore, we infected a triple dynamin knockout fibroblast cell line (characterized previously⁵⁰) as described above and counted how many protrusions were lysed during a 1-h time period. A minimum of 186 protrusions in at least 5 fields of view (295 μ m \times 295 μ m) were counted in four biological replicates between 8–13 hpi for both the dynamin positive (dnm+) and negative (dnm−) cell line. Similar to the dynasore treatment, 50% protrusion lysis was detected in dnm+ cells, whereas only 25% in the dnm− cells (Figure 4E, *t* test, $p = 0.0043$). To test whether dynamin knockout influences MNGC formation, we infected 40,000 dnm+ or dnm− cells at an MOI of 10. At 12 hpi, cells were fixed and Giemsa stained to visualize MNGC formation. We analyzed a minimum of 13 fields of view (295 μ m \times 295 μ m) and counted at least 1,000 nuclei for both the dnm+ and dnm− cell lines. As for the dynasore treatment, there was no significant difference in MNGC formation between the infection of dnm+ and dnm− cells (Figure 4F). In addition, no difference was detected in the size of plaques formed during infections of the dnm+ and dnm− cells (Figure S5B). Overall, both dynasore treatment and dynamin knockout decreased the rate of protrusion lysis by at least 2-fold; however, the rate of MNGC formation remained unaffected. Because MNGC formation is dependent on T6SS-5, which is activated predominantly in the protrusions, this suggests that the chance of MNGC formation upon T6SS-5-dependent protrusion lysis is higher without dynamin activity.

Dynamin-2 localizes to protrusions shortly before and after the T6SS-5 assembly

To further dissect the role of dynamin-2 in the cell-to-cell spread, we infected SK-MEL-2 cells expressing dynamin-2-GFP with both *S. flexneri* (MOI of 10, at 14–17 hpi) and *B. thailandensis* (MOI of 50, at 12–14 hpi) and imaged dynamin-2 localization. We show that dynamin-2 localized to protrusions formed by *S. flexneri* before their detachment from the rest of the host

cell membrane (Figure S5C). This indicated that dynamin-2 could be involved in this process as suggested previously.¹⁶ Subsequently, we investigated whether host cell protrusions formed by *B. thailandensis* also colocalized with dynamin-2. A total of 19 fields of view (295 μ m \times 295 μ m) in three biological replicates were analyzed. We identified 80 events of dynamin-2 localization to the host cell protrusions that contained *B. thailandensis* (Figures 4G and S6A; Video S5). Interestingly, 60 of the dynamin-2-GFP localization events were 30 pairs of sequential dynamin-2 localization events on the same protrusion (Figure 4H). Dynamin-2 first localized to the protrusion tail and caused its detachment from the host cell membrane. On average about 2 min (30–360 s) later, T6SS-5 assemblies were observed in the bacteria now residing in a detached protrusion (Figure S6B). This was followed by a second dynamin-2 localization event correlating with the lysis of the detached protrusion. Out of the 30 analyzed sequence of events, 20 of the second dynamin-2 localizations occurred in the same frame or 30 s after the T6SS-5 assembly event (Figure S6C). On average, the second dynamin-2 event occurred about 70 s after the T6SS-5 assembly event. Finally, we identified 98 bacteria in three biological replicates with detectable T6SS-5 assemblies and looked for dynamin-2 localization around the bacteria within 5 min before T6SS-5 assembly. Only 33 bacteria remained in focus for the entire 5 min period, and dynamin-2 localization was detected for 14 bacteria (42%). Overall, this correlation in dynamin-2 localization, T6SS-5 activity, and bacterial escape suggests that dynamin-2-mediated protrusion detachment could be a signal for T6SS-5 assembly and that dynamin-2 could also play a role in protrusion lysis or formation of membrane fragments after the protrusion lysis.

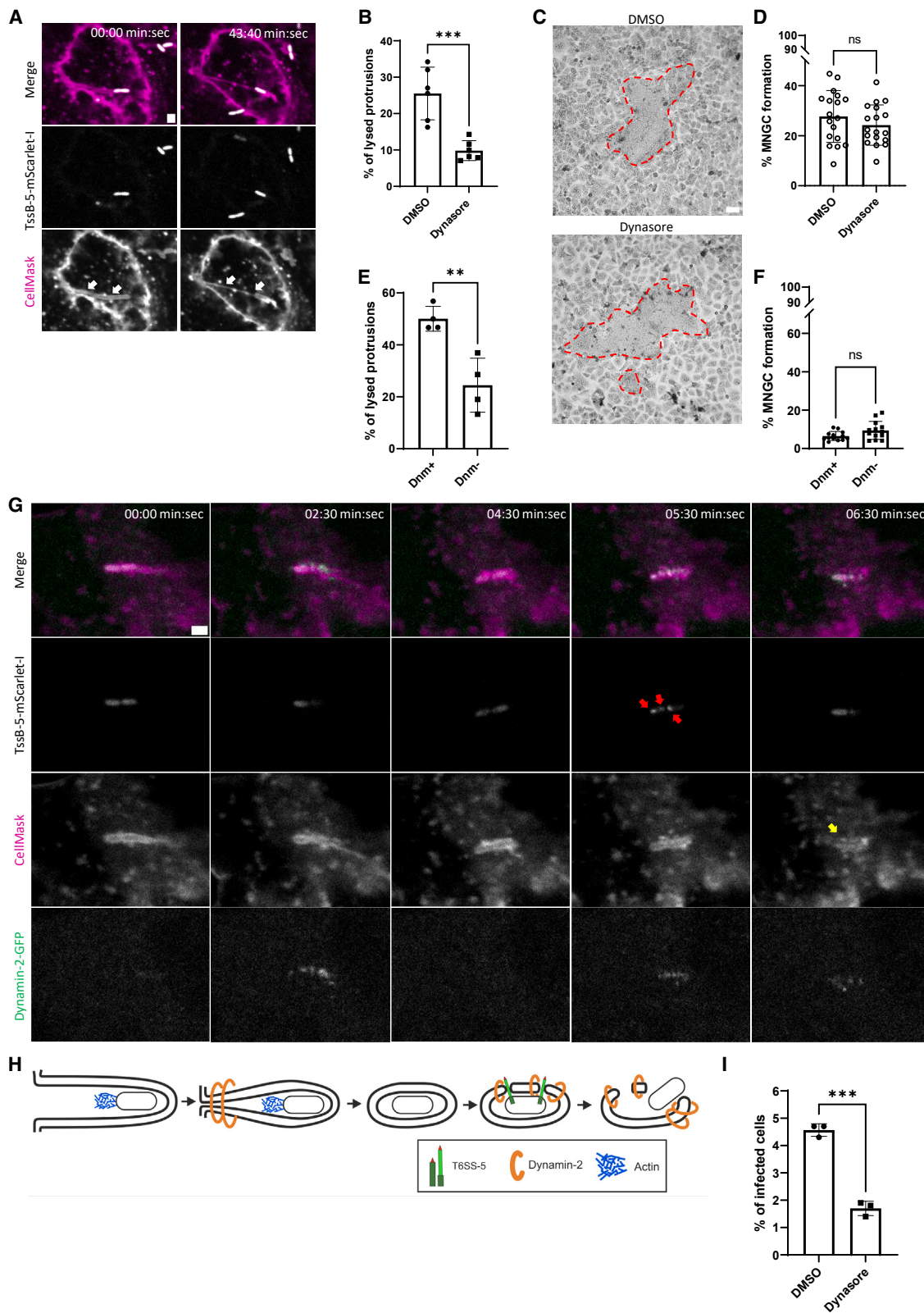
Dynamin is required for direct cell-cell spread

To investigate the role of dynamin in MNGC-formation-independent cell-cell spread, we quantified the number of infected cells using flow cytometry. A549 cells were infected at an MOI of 50 with the parental *B. thailandensis* TssB-5-mScarlet-I strain and either treated with 120 μ M dynasore or DMSO. At 12 hpi, the cells were trypsinized, fixed with 4% paraformaldehyde (PFA), and filtered through a 35- μ m filter to remove MNGCs. At least 300,000 events were analyzed per sample (three biological replicates) using the same gating strategy, and the infected cells were identified by detecting mScarlet-I fluorescence signal (Figures S7A–S7D). Less than 0.2% of uninfected cells were counted as mScarlet-I positive (Figure S7E). Importantly, this analysis showed that dynasore treatment lowered the fraction of infected cells by almost 3-fold from an average of 4.6% infected DMSO-treated cells to only 1.7% infected dynasore-treated cells (Figure 4I). Because we removed MNGCs, and the

Figure 3. T6SS-5-dependent lysis of protrusions leads to MNGC-independent cell-cell spread

(A) Example of protrusion lysis, which leads to MNGC formation. TssB-5-mScarlet-I *B. thailandensis*-infected HeLa cells (MOI 50). Host cell membranes (CellMask DeepRed, magenta), T6SS-5 (TssB-5-mScarlet-I, gray), and the cytoplasm (galectin-3-GFP, green). A magnified image (white box) of the bacteria that induced MNGC formation is shown underneath the merged image. Full time-lapse (from 10:40 hpi) in Video S4. Red arrows, T6SS-5 assembly; yellow arrows, host cell membrane lysis. The scale bar represents 10 μ m (4 μ m for the magnified image).
(B) Example of protrusion lysis without MNGC formation. A549 cells infected with TssB-5-mScarlet-I *B. thailandensis* (MOI 50). The scale bar represents 5 μ m. The magnified image shows the escape of the bacterium from the protrusion at 0 and 1:30 min. The CellMask panel shows no MNGC formation at the 9:30 min mark. Time-lapse (from 14:40 hpi) in Video S4.

See also Figure S4.



(legend on next page)

12 h infection was performed in the presence of kanamycin to prevent reinfection, the cells containing bacteria had to be predominantly infected due to direct spread from cell to cell. These results therefore indicate that dynamin activity increases MNGC-independent cell-cell spread.

New actin tail formation occurs before detectable protrusion lysis

To understand how actin tail formation contributes to protrusion lysis and escape of bacteria from membrane fragments, we transfected A549 lung cells with a Lifeact-eGFP-expressing plasmid, stained the host cell membrane with CM, and infected them with the *B. thailandensis* TssB-5-mScarlet-I strain. We focused on bacterial protrusions from non-transfected cells into Lifeact-eGFP expressing cells. We investigated 16 protrusion lysis events in three biological replicates. Interestingly, we observed that T6SS-5 assembly events were directly followed by localization of labeled actin either around the bacterium or next to one bacterial pole in the form of actin tails. We often observed actin localized around the bacterium and later relocating to one bacterial pole (Figure S8A). The localization of actin occurred in 13 out of 15 cases within 30–60 s and in 2 cases within 5 or 11 min, after T6SS-5 assembly. Interestingly, in 13 cases, it took less than 90 s from actin polymerization to detectable lysis of the host cell protrusions and membrane fragmentation, although in 2 cases, it took up to 10 min (Figures 5A, S8A, and S8B; Video S6). This suggests that T6SS-5 disrupts the host cell membranes, which allows actin to diffuse into the protrusion from the newly invaded host cell, and actin tail formation may contribute to complete protrusion lysis (Figure 5B).

Galectin-3 fails to recognize membranes lysed by T6SS-5

The host protein galectin-3 binds to β -galactosides commonly found on the extracellular surface of the host cell membranes, and its relocation can be used to detect membrane disruption events.^{51–53} To assess the mechanism of protrusion

lysis, we infected galectin-3-GFP-expressing HeLa cells with either the *B. thailandensis* parental strain or T6SS-5-negative *B. thailandensis* (*hcp-5* or *vgrG-5* deletion). As a control, we infected the cells with *S. flexneri*, which is known to expose the extra-cellular-membrane-bound β -galactosides to the cytoplasmic galectin-3 during protrusion lysis.⁵³ To localize the bacteria during infection, *B. thailandensis* strains were expressing mCherry2 from a neutral chromosomal site, and *S. flexneri* was expressing dsRed from a plasmid. For each strain, we analyzed single frames from a time-lapse collected between 12:30 and 16:00 hpi for at least 106 fields of view (295 μm \times 295 μm) and counted how many galectin-3 accumulation events were present per 1,000 bacteria (at least 22,286 bacteria per strain in at least four biological replicates). During *S. flexneri* infections, we identified on average 213 galectin-3 accumulations per 1,000 bacteria (Figures 6A, and 6B; Video S7). Surprisingly, during infections by *B. thailandensis* T6SS-5-positive strain, we detected on average only 7 accumulation events of galectin-3 per 1,000 bacteria (Figures 6A, and 6B; Video S7). On the other hand, during the infections with the T6SS-5 negative *B. thailandensis*, we counted on average 48 ($\Delta hcp-5$) and 40 ($\Delta vgrG-5$) galectin-3 accumulation events per 1,000 bacteria (Figures 6A, 6B, and S9A; Video S7).

To determine whether galectin-3 accumulates to host cell membranes during protrusion escape, we reanalyzed the dataset described above where galectin-3-GFP-expressing HeLa cells were infected with the TssB-5-mScarlet-I strain or with the *hcp-5/vgrG-5*-negative TssB-5-mScarlet-I strain. In 22 fields of view (81 μm \times 81 μm) we counted the number of protrusion lysis events that showed galectin-3 accumulations. For the T6SS-5-positive strain, we observed 91 protrusion lysis events during a 1-h period, and only 3 (3.3%) were colocalized with galectin-3 (Figures 6C, 6D, 6G, and S9B; Video S8). In contrast, we recorded 23 protrusion lysis events for the T6SS-5-negative mutant, of which 14 (61%) showed a galectin-3 accumulation (Figures 6E–6G and S9C; Video S8). Overall, this analysis shows that T6SS-5 allows *B. thailandensis* to lyse cell membranes without the recruitment of galectin-3, suggesting that it could

Figure 4. Role of dynamin-2 in *B. thailandensis* protrusion lysis

- (A) An example of a long intact protrusion detected after treatment with 120 μM dynasore. A549 cells infected (MOI 50) with *B. thailandensis* TssB-5-mScarlet-I. Imaging from 16 hpi for 1 h. White arrows indicate the protrusion in the CellMask DeepRed (magenta) channel. Scale bar represents 2 μm .
- (B) Percentage of dynasore-treated protrusions lysed during a 1-h period. A549 cells infected as in (A). Untreated: 508 protrusions in 6 fields of view (295 μm \times 295 μm). Dynasore treated: 523 protrusions in 6 fields of view (295 μm \times 295 μm). Imaging between 13:30–15:30 hpi 1 h after the dynasore treatment. Data from two biological replicates, a two-tailed unpaired t test used (** p < 0.001).
- (C) MNGC formation analyzed by Giemsa stain. Cells infected as in (A). Cells stained at 16 hpi. Dotted red line indicates MNGCs. Scale bar, 50 μm .
- (D) Giemsa stain analysis of dynasore- and DMSO-treated cells. MNGC formation is shown as a percentage of the total number of nuclei compared with the number of nuclei in MNGCs. At least 18 random fields of view with at least 4,300 nuclei were analyzed. A two-tailed unpaired t test was performed (ns: not significant).
- (E) The percentage of protrusion lysis during an infection of dynamin positive (dnm+) and negative (dnm-) mouse fibroblasts. Infection (MOI 10) imaged at 8–13 hpi. At least 180 protrusions were counted in 5 fields of view (295 μm \times 295 μm). Four biological replicates, a two-tailed unpaired t test (ns: not significant).
- (F) Giemsa stain analysis of dynamin-positive (dnm+) and -negative (dnm-) cells. MNGC formation as a percentage of total number of nuclei compared with the number of nuclei in MNGCs. At least 13 random fields of view with at least 960 nuclei were analyzed. A two-tailed unpaired t test was performed (** p < 0.005).
- (G) SK-MEL-2 cells expressing dynamin-2-GFP were infected with *B. thailandensis* TssB-5-mScarlet-I (MOI 50). The merged images on the top show T6SS-5 (TssB-5-mScarlet-I, grayscale), host cell membranes (CellMask DeepRed, magenta), and dynamin-2-GFP (green); channels are shown separately below. The red arrows indicate T6SS-5 assemblies, and the yellow arrow indicates protrusion lysis. Imaging at 14 hpi; full time-lapse in Video S5. Scale bar represents 2 μm .
- (H) Scheme of the mode of action of dynamin-2. *B. thailandensis* forms a protrusion, dynamin-2 localizes to the protrusion and detaches the protrusion. T6SS-5 assemblies cause membrane fragmentation that recruits dynamin-2.
- (I) Percentage of infected A549 cells (identified by flow cytometry upon removal of MNGCs). Cells infected (MOI 50) with the parental strain and treated with dynasore or DMSO. Cells fixed at 12 hpi with PFA, at least 300,000 events recorded in three biological replicates. A two-tailed unpaired t test was performed (** p < 0.001).

See also Figures S5, S6, and S7.

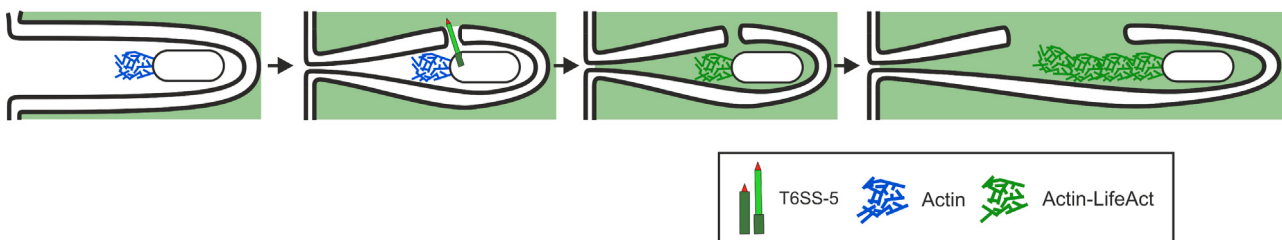
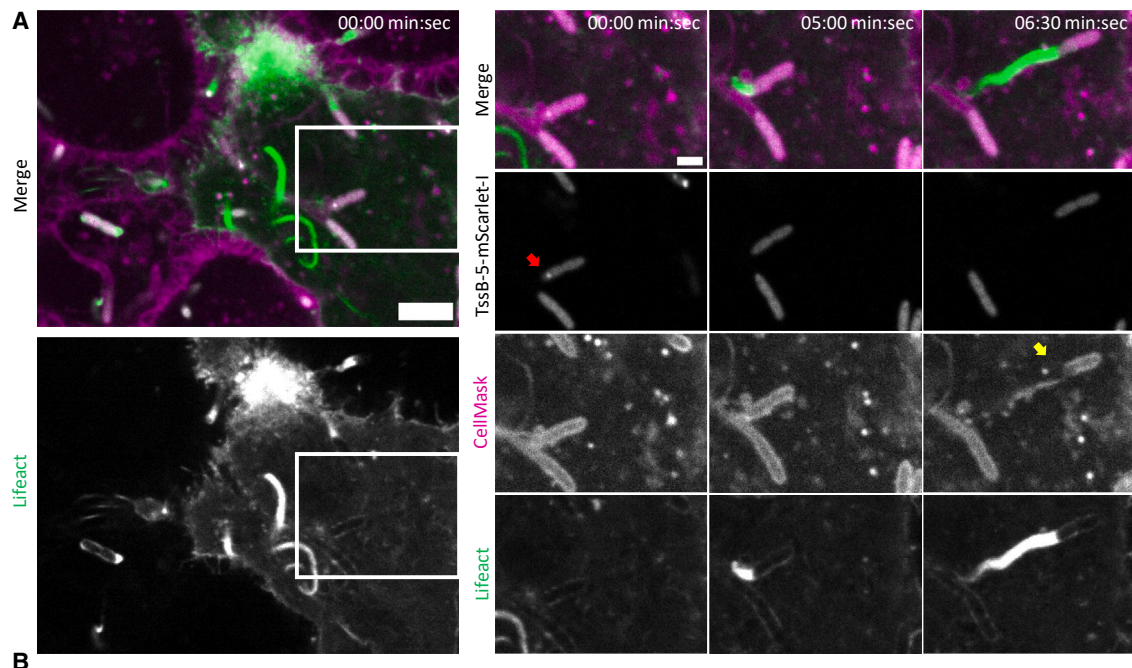


Figure 5. Actin tail formation occurs before complete protrusion lysis

(A) HeLa-CCL2 cells transfected with Lifeact-eGFP were infected with TssB-5-mScarlet-I *B. thailandensis* (MOI 50). The merged images on the top show T6SS-5 (TssB-5-mScarlet-I, grayscale), host cell membranes (CellMask DeepRed, magenta), and F-actin (Lifeact-eGFP, green); individual channels shown below in grayscale. The red arrow indicates T6SS-5 assembly; the yellow arrow indicates protrusion lysis. The images were taken at 15 hpi and show an overview (on the left) and three-time points (on the right), full time-lapse in [Video S6](#). Scale bars represent 2 μ m in the magnified image and 5 μ m in the overview image.

(B) Illustration of a protrusion lysis, one cell has actin labeled, and one is unlabeled. A T6SS-5 assembly and the subsequent membrane damage in the protrusion cause the influx of actin from the actin-labeled cell, which allows the formation of a labeled actin tail.

See also [Figure S8](#).

spread from cell to cell without triggering the host cell membrane lysis detection mechanisms.

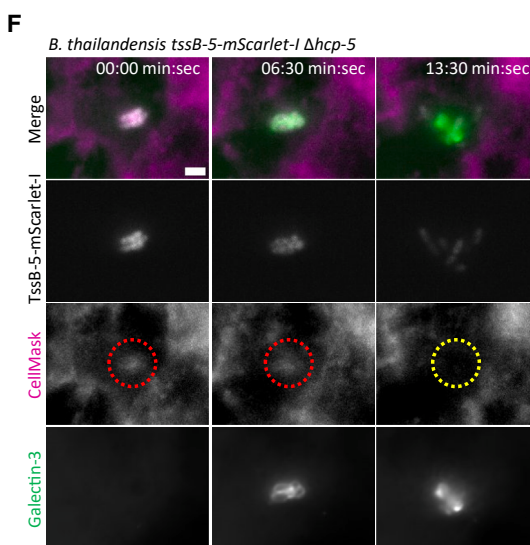
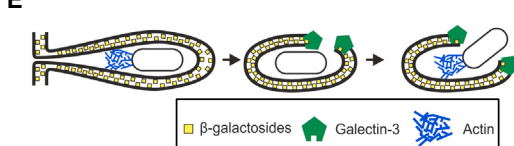
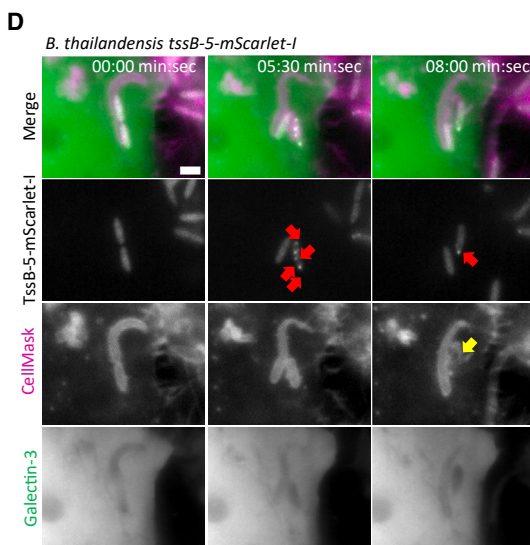
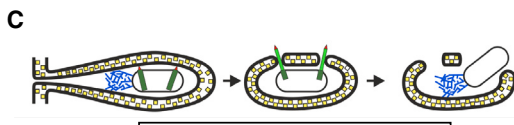
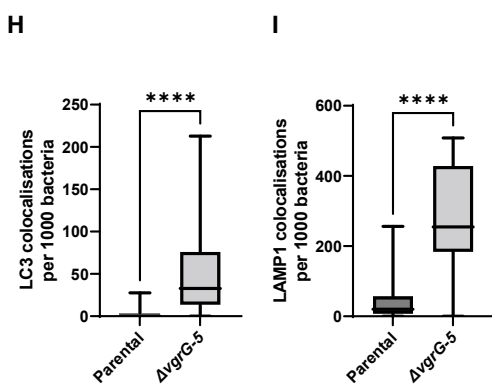
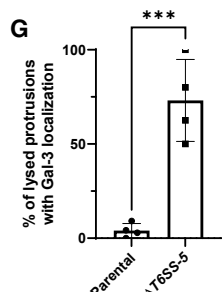
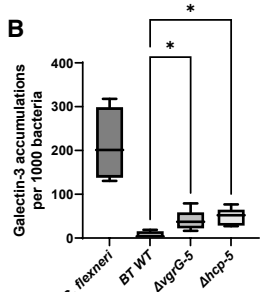
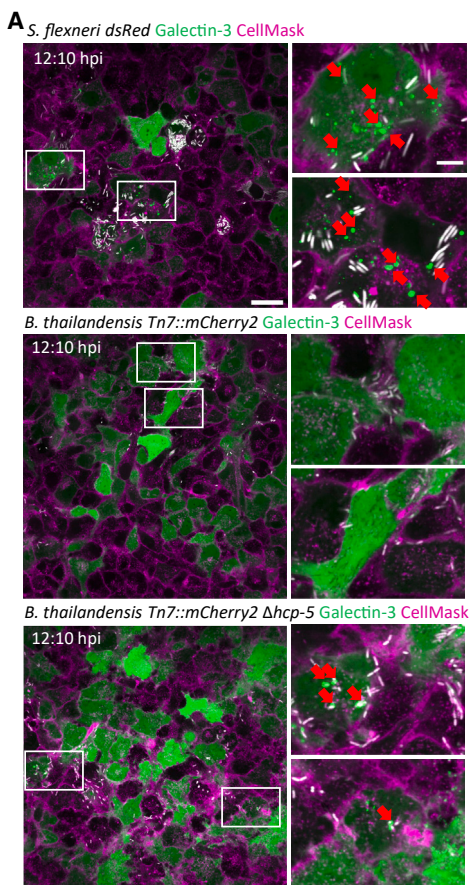
T6SS-5 activity lowers the colocalization of bacteria with LC3 and LAMP1

To explore the potential connection between reduced galectin-3 localization and downstream processes during *B. thailandensis* infections, we analyzed the localization of the autophagic marker protein LC3 and the lysosomal marker LAMP1. We infected HeLa cells with either the parental TssB-5-mScarlet-I *B. thailandensis* strain or one of the two T6SS-5-negative strains (Δ vgrG-5 and Δ hcp-5) at an MOI of 100. The host cells were fixed and permeabilized at 17 hpi with 100% methanol and stained with an antibody against LC3B or LAMP1. The autophagy-inducing compound chloroquine diphosphate was used as a positive control for the LC3B antibody. Colocalization of bacteria with LC3B or LAMP1 was analyzed for at least 2,100 bacteria in 24 fields of view

(295 μ m \times 295 μ m) per strain in three biological replicates ([Figures 6H, 6I, and S9D](#)). The parental strain showed on average only 4 LC3 colocalization events per 1,000 bacteria, whereas 53 events per 1,000 bacteria were detected for the T6SS-5-negative strain. Similarly, the parental strain showed only 44 LAMP1 colocalization events per 1,000 bacteria, whereas 288 events were detected per 1,000 bacteria for the T6SS-5-negative strain. In summary, LC3 and LAMP1 colocalization occurred less frequently with the T6SS-5-positive strain than with the T6SS-5-negative strain, similar to the difference observed for galectin-3 localization. This suggests that T6SS-5 activity lowers recognition of *B. thailandensis* by cell-autonomous immunity systems.

DISCUSSION

We show here that during cell-to-cell spread, *B. thailandensis* generates membrane protrusions and lyses them with T6SS-5.



(legend on next page)

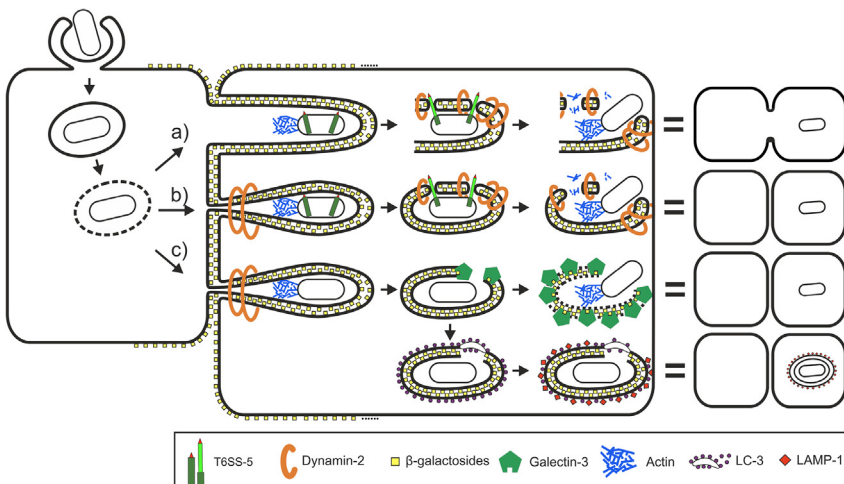
Interestingly, the assembly of the T6SS-5 is specifically triggered when the bacteria are in direct contact with host membranes or in protrusions. In previous studies, it was observed that T6SS-5 expression is upregulated after *B. thailandensis* escapes in a T3SS-dependent manner from the primary vacuole^{10,11} and that dynamic ClpV-5 foci localized to the bacterial pole, suggesting that T6SS-5 assembly is mostly polar.¹⁷ In addition, it was shown that *B. thailandensis* can form membrane protrusions from one host cell to another while polymerizing actin.^{12,13} Here, we show that the sheath of *B. thailandensis* T6SS-5 undergoes expected cycles of assembly and disassembly and that the assembly preferentially localizes to the bacterial pole (Figures 1B and S1F; Video S1). Furthermore, we show that the four T6SS-5-associated genes (*tagAB-5*, *tagB-5*, *tagC-5*, and *tagD-5*) are required for T6SS-5 assembly (Figure S1H), explaining why *B. pseudomallei* mutants lacking TagAB-5 are attenuated in mouse models.⁴⁰ Surprisingly, we show that only a subset of bacteria assembles T6SS-5 at any given time point (Figure 2B). More specifically, our imaging of the host membrane and T6SS-5 dynamics showed that 80% of observed T6SS-5 assemblies take place inside of host cell membrane protrusions (Figure 2B). This suggests that *B. thailandensis* evolved to precisely initiate T6SS-5 assembly to increase the likelihood of targeting the host membrane. This is consistent with the fact that host cell-cell fusion (MNGC formation) was proposed to be mediated by direct translocation of the VgrG-5 CTD across the membranes of two neighboring cells.³⁵ How *B. thailandensis* triggers T6SS-5 assembly is unclear; however, it could sense tight contact with the host membrane or increased pressure or may have the ability to detect host membrane proteins, such as tetraspanins, or respond to cholesterol-rich membrane rafts, which were shown to be required for MNGC formation.^{54,55} Interestingly, post-translational regulation of the T6SS assembly was also shown for H1-T6SS of *Pseudomonas aeruginosa*^{56–58} and the anti-bacterial T6SS of *Acinetobacter* and *B. thailandensis* (T6SS-1).⁵⁹

We show that during a long-term infection, bacteria are also present in the host cells surrounding MNGCs, indicating that only some protrusion lysis events result in MNGC formation (Figures 1D and S2; Video S2). Indeed, we estimated that one in six protrusion lysis events were followed by cell-cell fusion (Figure 3A; Video S4); however, precise quantification is challenging because multiple protrusions form between neighboring cells (Figure S4A). Nevertheless, this was unexpected because MNGC formation was described as the primary mechanism of intercellular spread for *B. thailandensis*.^{9,11} In addition, it is interesting that the *B. thailandensis* T6SS-5-negative strain can escape from protrusions, albeit at low frequency, and thus slowly spread without causing MNGCs (Figures 2D and 2F; Video S2).

MNGC formation was described in numerous *Burkholderia* strains and various cell lines,⁹ as well as in several patients with *B. pseudomallei* infection.^{60,61} However, the overall level of MNGC formation may be limited due to the activation of the pyroptotic cell death by the intracellular bacteria upon IFN- γ stimulation, as shown for the less virulent *B. thailandensis*.¹⁸ Nevertheless, MNGC formation could be a survival strategy during chronic infections, allowing bacteria to avoid the host immune response.^{60–63} MNGC formation also allows the spread of many bacteria within the tissue compared with the transfer of only one or two bacteria during a protrusion lysis event. Finally, the eventual release of a large number of bacteria from a lysed MNGC could overwhelm the extracellular immune system and allow better survival and dissemination. On the other hand, MNGC formation was also shown to cause host cell lysis via induction of the cGAS-STING pathway due to aberrant cell division and the presence of micronuclei, causing increased pathogenesis in the mouse chronic infection model.⁶⁴ This suggests that direct T6SS-5-dependent lysis of protrusions could be a mechanism to avoid the acute pro-inflammatory immune response to MNGC formation while facilitating the efficient dissemination and spread of bacteria.

Figure 6. T6SS-5-dependent protrusion lysis fails to induce galectin-3 localization

- (A) Galectin-3 localization during infection. Galectin-3-GFP-expressing HeLa-CCL2 cells were infected with either *S. flexneri* M90t-expressing DsRed (MOI 10), *B. thailandensis* expressing mCherry2 (MOI 100), or *B. thailandensis* Δ hcp-5-expressing mCherry2 (MOI 100). Host cell membranes were stained with CellMask DeepRed. Images shown were taken at 12:10 hpi, full time-lapse (from 3:40 to 19:10 hpi every 30 min) in Video S7. The green foci (red arrows) in the magnified panels (white box) show galectin-3 accumulation events. Scale bars represent 5 μ m in the magnified panel and 30 μ m in the overview image.
 - (B) Number of galectin-3-GFP accumulations detected per 1,000 bacteria (background removed based on analysis of uninfected cells). Images were acquired at 12:30 to 16 hpi, and at least 106 fields of view (295 μ m \times 295 μ m) were analyzed per strain. One-way ANOVA was carried out to determine the statistical significance (* $p < 0.05$).
 - (C) Illustration of the proposed model for a protrusion lysis event in which galectin-3 fails to localize to the lysed protrusion.
 - (D) Galectin-3-GFP-expressing HeLa-CCL2 cells infected with *B. thailandensis* TssB-5-mScarlet-I (MOI 50). The merge image shows TssB-5-mScarlet-I (gray), galectin-3-GFP (green), and the host membrane (CellMask DeepRed, magenta), images underneath show the indicated channels in grayscale. Full time-lapse (taken from 10:40 hpi) in Video S8. Scale bar represents 2 μ m.
 - (E) Illustration of the proposed model in which a T6SS-5-negative *B. thailandensis* strain causes a galectin-3 localization event.
 - (F) Galectin-3-GFP HeLa-CCL2 cells infected with *B. thailandensis* Δ hcp-5 TssB-5-mScarlet-I (MOI 50). Images as in (D). Red dotted circle shows intact host cell membranes, and the yellow dotted circle shows the disappearance of the host cell membrane. Full time-lapse (from 11 hpi) in Video S8. Scale bar represents 2 μ m.
 - (G) Quantification of protrusion lysis and galectin-3-GFP localization during 1-h imaging. HeLa cells infected (MOI 50) with either *B. thailandensis* TssB-5-mScarlet-I parental strain or the indicated Δ T6SS-5 strains. Parental strain: 22 fields of view (81 μ m \times 81 μ m), Δ T6SS-5 strains: 35 fields of view (81 μ m \times 81 μ m). Four biological replicates for each strain, two-tailed unpaired t test used (** $p < 0.001$).
 - (H) Quantification of colocalizations of LC3B with *B. thailandensis* (HeLa cells, 17 hpi, MOI 100). At least 2,100 bacteria were counted per strain in 24 fields of view (295 μ m \times 295 μ m). Three biological replicates, and a two-tailed unpaired t test used (**** $p < 0.0001$).
 - (I) LAMP1 colocalizations with *B. thailandensis* parental and Δ vgrG-5 strains (HeLa cells, 17 hpi, MOI 100). At least 2,100 bacteria and the corresponding LAMP1 colocalizations were counted in 24 fields of view (295 μ m \times 295 μ m). Three biological replicates, and a two-tailed unpaired t test used (**** $p < 0.0001$).
- See also Figure S9.



cell. T6SS-5 assembly is triggered by tight contact with host cell membranes or other unknown signals. The exposed β -galactosides to galectin-3. Subsequently, dynamin-2 attaches to the membrane remnants. Actin influx allows the formation of new actin tails. Because the protrusion was detached by the first dynamin-2 event, no MNGC formation is induced, and only direct cell-cell spread occurs. (C) Protrusion collapses, and dynamin-2 detaches it from the initially infected cell. In rare cases, no T6SS-5 events occur, and *B. thailandensis* lyses the detached protrusion via an unknown mechanism, which causes the formation of new actin tails and the spread from cell to cell. This T6SS-5 independent escape exposes the β -galactosides to galectin-3 and subsequently leads to the recruitment of LC3 and LAMP1.

T6SS-5 assembly often happens in short bursts when the bacteria are in membrane protrusions away from the host cell contact sites, suggesting that a specific signal triggers T6SS-5 assembly. Interestingly, previous studies indicated that dynamin-2 binds presumably to the membranes around actin tails of *S. flexneri*, and it was proposed that dynamin-2 is involved in dissemination into neighboring cells.¹⁶ Importantly, the curvature of host cell membranes alone can cause dynamin recruitment.^{65,66} Our time-lapse imaging showed that dynamin-2 localization to the membrane protrusions and the protrusion detachment from the host cell membrane correlated with bursts of T6SS-5 activity (Figures 4G and S6A; Video S5). T6SS-5 activity was quickly followed by the influx of actin monomers from the neighboring host cell and the formation of new actin tails, even before membrane fragmentation and protrusion lysis were detectable (Figures 5A, S8A, and S8B; Video S6). Membrane fragmentation correlated with further dynamin-2 recruitment (Figures 4G and S6A; Video S5). This suggests that dynamin-2 could be first recruited when the protrusion diameter becomes small, and subsequent T6SS-5 activity would generate small membrane vesicles that would further recruit dynamin-2. Interestingly, for *S. flexneri*, we only detected dynamin-2 at the membrane protrusion during detachment from the host cell membrane (Figure S5C), suggesting that membrane lysis by those two bacteria is achieved by fundamentally different mechanisms. Importantly, despite the observed dynamic localization of dynamin-2-GFP and dynamin-2 being the prevalent isoform in all cell types, except for neurons and testis,^{50,67,68} we cannot exclude that other dynamin isoforms or other host factors are required for protrusion lysis and cell-cell spread.

Interestingly, we show that dynamin inhibition has no impact on MNGC formation and plaque size (Figures 4C, 4D, 4F, and S5B). This is consistent with the fact that MNGCs are the precursors for the formation of plaques during *B. thailandensis* infec-

Figure 7. Model of *B. thailandensis* spread from cell to cell

B. thailandensis enters the primary host cell, escapes from the vacuole by utilizing its T3SS_{Bsa}, and then polymerizes actin tails (blue) to form membrane protrusions. In our proposed model, there are three modes of cell-to-cell spread.

(A) *B. thailandensis* senses the membrane protrusion and fires T6SS-5 (light and dark green tube) before the protrusion collapses and is detached from the host cell. The double membrane protrusion is lysed in a way that avoids the exposure of β -galactosides (yellow) to galectin-3 (green hexagons), thus avoiding host cell recognition. Dynamin-2 then binds to the membrane remnants and actin (blue) influx from the new host cell allows the formation of new actin tails. The host cell is unable to repair the damaged membranes, and the membranes fuse leading to MNGC formation.

(B) Protrusion collapses, dynamin-2 binds to the collapsed protrusion and detaches it from the host

cell. T6SS-5 assembly is triggered by tight contact with host cell membranes or other unknown signals. The exposed β -galactosides to galectin-3. Subsequently, dynamin-2 attaches to the membrane remnants. Actin influx allows the formation of new actin tails. Because the protrusion was detached by the first dynamin-2 event, no MNGC formation is induced, and only direct cell-cell spread occurs. (C) Protrusion collapses, and dynamin-2 detaches it from the initially infected cell. In rare cases, no T6SS-5 events occur, and *B. thailandensis* lyses the detached protrusion via an unknown mechanism, which causes the formation of new actin tails and the spread from cell to cell. This T6SS-5 independent escape exposes the β -galactosides to galectin-3 and subsequently leads to the recruitment of LC3 and LAMP1.

tions.¹¹ In contrast, dynasore treatment lowers plaque formation during *S. flexneri* infections.⁴⁸ However, direct bacterial cell-cell spread is potentially undetected during standard MNGC formation and plaque assays. Indeed, we show that protrusion lysis by *B. thailandensis* in dynasore-treated A549 cells or dynamin knockout cell lines is significantly reduced (Figures 4B and 4E), correlating with a lower rate of cell-cell spread beyond MNGCs in dynasore-inhibited cells (Figure 4I).

Cell-cell fusion, and thus MNGC formation, can be only achieved if T6SS-5 activity is triggered before the protrusion is detached from the cell membrane and the bacterium appears in a double membrane vacuole (Figure 7). Interestingly, because MNGC formation is sensed by innate immunity and results in host cell death, our data suggest that *B. thailandensis* potentially evolved a mechanism to lower the rate of MNGC formation by preferentially activating T6SS-5 only after detachment of the protrusions from the cell membrane (Figures 7 and S6B). Although the overall rate of MNGC formation is independent of dynamin, the rate at which individual protrusion lysis events result in cell-cell fusion is actually increased in the absence of dynamin activity. This is because the overall rate of protrusion lysis is lower when dynamin is inactivated (Figures 4B and 4E); thus, fewer protrusion lysis events are needed for the same number of cell-cell fusion events.

One of the mechanisms of how host cells sense intracellular pathogens is the binding and localization of galectin-3 to β -galactosides exposed to the cytoplasm upon cell membrane lysis. Accumulation of galectin-3 can induce either the membrane repair mechanism by the ESCRT machinery or the recruitment of LC3 and LAMP1 resulting in the degradation of the membranes and bacterial killing.^{69–71} Most studies for *B. thailandensis* or *B. pseudomallei* focused on the early stages of infection in which LC3 localizes to primary vacuoles disrupted by *Burkholderia* in a T3SS-dependent manner.⁷² However, β -galactosides are also found in between the host cell membranes in membrane

protrusions^{53,73}; therefore, we tested galectin-3, LC3, and LAMP1 localization in the later stages of infection when *B. thailandensis* spreads from one host cell to another. Surprisingly, we show that galectin-3 fails to recognize the membrane protrusions lysed in a T6SS-5-dependent manner and that active T6SS-5 lowers colocalization of bacteria with LC3 or LAMP1 (Figures 6 and S9; Video S7). This indicates that β-galactosides in the host membrane around the bacteria have no contact with cytoplasmic galectin-3 or that such interaction is prevented by an unknown mechanism.

It was proposed that VgrG-5 could act similar to viral-like fusogens,^{17,35} which cause a hemifusion of two membranes that resolves in membrane fusion.^{74–76} Therefore, VgrG-5 could cause a hemifusion of the two host cell membranes and thus prevent exposure of the β-galactosides to the cytoplasm of either host cell (Figure 7). The membrane fusion would then either resolve as a protrusion escape or lead to MNGC formation. The ability to avoid immunity signaling downstream of galectin-3 could allow *B. thailandensis* to spread inside a host organism without detection. This is in contrast to *L. monocytogenes* and *S. flexneri*, which lyse protrusions by mechanisms that trigger galectin-3 accumulation.⁵³ *L. monocytogenes* secretes listeriolysin O, which is a pore-forming toxin, and *S. flexneri* uses a T3SS to secrete several effectors that cause lysis of the engulfed protrusion.^{77–81} Surprisingly, we also show that when *B. thailandensis* lacks T6SS-5, it lyses the protrusions at a lower rate by an unknown mechanism, which triggers recognition by galectin-3 (Figure 6F). Moreover, the T6SS-5-negative strain colocalized with LC3 or LAMP1 more frequently than the T6SS-5-positive strain (Figures 6H and 6I).

In conclusion, our data demonstrate that *B. thailandensis* tightly regulates T6SS-5 assembly to spread from cell to cell by a mechanism that is independent of MNGC formation and allows membrane disruption by a unique mechanism to potentially minimize detection by the host immune system.

STAR METHODS

Detailed methods are provided in the online version of this paper and include the following:

- KEY RESOURCES TABLE

- RESOURCE AVAILABILITY

- Lead contact
- Materials availability
- Data and code availability

- EXPERIMENTAL MODEL AND STUDY PARTICIPANT DETAILS

- Bacterial strains, plasmids, and culturing conditions
- Mammalian cell lines and culturing

- METHOD DETAILS

- Infection assays
- Flow cytometry
- Transfection
- Giemsa stain and MNGC formation
- Plaque assay
- Counting of galectin-3 accumulations
- Immunofluorescence
- Live-cell confocal microscopy

- QUANTIFICATION AND STATISTICAL ANALYSIS

SUPPLEMENTAL INFORMATION

Supplemental information can be found online at <https://doi.org/10.1016/j.chom.2024.03.013>.

ACKNOWLEDGMENTS

This study was supported by the European Research Council consolidator grant (865105, “AimingT6SS”), and the University of Basel. The authors thank J.W.K. Ku (National University of Singapore) for advice; P. Broz and M. Dilucca (University of Lausanne) for the Lifeact-eGFP plasmid and guidance; A. Roux and C. Silvestre (University of Geneva) for the dynamin-2-GFP cells and advice in regard to dynamin; C. Dehio, I. Sorg, and J. Sedzicki (University of Basel) for the HeLa cell lines, lab space, and support; U. Jenal and B. Laventie (University of Basel) for providing plasmids and A549 cells; P. De Camilli and A. Vulpe (Yale University) for the TKO dynamin cell lines; L. Guerard and the IMCF (University of Basel) for support with the image analysis and acquisition; and Stella Stefanova and the FACS Core Facility (University of Basel) for support with the flow cytometry analysis.

AUTHOR CONTRIBUTIONS

Conceptualization, M.T.W.P. and M.B.; methodology, M.T.W.P., H.C.C., and P.R.I.; investigation, M.T.W.P., H.C.C., and P.R.I.; writing—original draft, M.T.W.P. and M.B.; writing—review and editing, M.T.W.P., H.C.C., and M.B.; funding acquisition, M.B.; resources, M.T.W.P. and Y.C.; supervision, Y.-H.G. and M.B.

DECLARATION OF INTERESTS

The authors declare no competing interests.

Received: March 1, 2023

Revised: August 1, 2023

Accepted: March 27, 2024

Published: April 18, 2024

REFERENCES

1. Currie, B.J., Fisher, D.A., Howard, D.M., Burrow, J.N.C., Selvanayagam, S., Snelling, P.L., Anstey, N.M., and Mayo, M.J. (2000). The epidemiology of melioidosis in Australia and Papua New Guinea. *Acta Trop.* 74, 121–127. [https://doi.org/10.1016/S0001-706X\(99\)00060-1](https://doi.org/10.1016/S0001-706X(99)00060-1).
2. Limmathurotsakul, D., Golding, N., Dance, D.A.B., Messina, J.P., Pigott, D.M., Moyes, C.L., Rolim, D.B., Bertherat, E., Day, N.P.J., Peacock, S.J., and Hay, S.I. (2016). Predicted global distribution of *Burkholderia pseudomallei* and burden of melioidosis. *Nat. Microbiol.* 1, 15008. <https://doi.org/10.1038/nmicrobiol.2015.8>.
3. Limmathurotsakul, D., Wongratanacheewin, S., Teerawattanasook, N., Wongsuphan, G., Chaisuksant, S., Chetchotisakd, P., Chaowagul, W., Day, N.P., and Peacock, S.J. (2010). Increasing Incidence of Human Melioidosis in Northeast Thailand. *Am. J. Trop. Med. Hyg.* 82, 1113–1117. <https://doi.org/10.4269/ajtmh.2010.10-0038>.
4. Barnes, J.L., and Ketheesan, N. (2005). Route of Infection in Melioidosis. *Emerg. Infect. Dis.* 11, 638–639. <https://doi.org/10.3201/eid1104.041051>.
5. Sanchez-Villamil, J.I., Tapia, D., Borlee, G.I., Borlee, B.R., Walker, D.H., and Torres, A.G. (2020). *Burkholderia pseudomallei* as an Enteric Pathogen: Identification of Virulence Factors Mediating Gastrointestinal Infection. *Infect. Immun.* 89, e00654-20. <https://doi.org/10.1128/IAI.00654-20>.
6. Rhodes, K.A., and Schweizer, H.P. (2016). Antibiotic resistance in *Burkholderia* species. *Drug Resist. Updat.* 28, 82–90. <https://doi.org/10.1016/j.drup.2016.07.003>.
7. Fisher, N.A., Ribot, W.J., Applefeld, W., and DeShazer, D. (2012). The Madagascar hissing cockroach as a novel surrogate host for *Burkholderia pseudomallei*, *B. mallei* and *B. thailandensis*. *BMC Microbiol.* 12, 117. <https://doi.org/10.1186/1471-2180-12-117>.

8. West, T.E., Frevert, C.W., Liggitt, H.D., and Skerrett, S.J. (2008). Inhalation of *Burkholderia thailandensis* results in lethal necrotizing pneumonia in mice: a surrogate model for pneumonic melioidosis. *Trans. R. Soc. Trop. Med. Hyg.* 102, S119–S126. [https://doi.org/10.1016/S0035-9203\(08\)70028-2](https://doi.org/10.1016/S0035-9203(08)70028-2).
9. Whiteley, L., Meffert, T., Haug, M., Weidenmaier, C., Hopf, V., Bitschar, K., Schittekk, B., Kohler, C., Steinmetz, I., West, T.E., and Schwarz, S. (2017). Entry, Intracellular Survival, and Multinucleated-Giant-Cell-Forming Activity of *Burkholderia pseudomallei* in Human Primary Phagocytic and Nonphagocytic Cells. *Infect. Immun.* 85, e00468–17. <https://doi.org/10.1128/IAI.00468-17>.
10. Burnick, M.N., Brett, P.J., Nair, V., Warawa, J.M., Woods, D.E., and Gherardini, F.C. (2008). *Burkholderia pseudomallei* Type III Secretion System Mutants Exhibit Delayed Vacuolar Escape Phenotypes in RAW 264.7 Murine Macrophages. *Infect. Immun.* 76, 2991–3000. <https://doi.org/10.1128/IAI.00263-08>.
11. French, C.T., Toesca, I.J., Wu, T.-H., Teslaa, T., Beaty, S.M., Wong, W., Liu, M., Schröder, I., Chiou, P.-Y., Teitel, M.A., and Miller, J.F. (2011). Dissection of the *Burkholderia* intracellular life cycle using a photothermal nanoblade. *Proc. Natl. Acad. Sci. USA* 108, 12095–12100. <https://doi.org/10.1073/pnas.1107183108>.
12. Benanti, E.L., Nguyen, C.M., and Welch, M.D. (2015). Virulent *Burkholderia* species Mimic Host Actin Polymerases to Drive Actin-Based Motility. *Cell* 161, 348–360. <https://doi.org/10.1016/j.cell.2015.02.044>.
13. Kesphichayawattana, W., Rattanachetkul, S., Wanun, T., Utasincharoen, P., and Sirisinha, S. (2000). *Burkholderia pseudomallei* Induces Cell Fusion and Actin-Associated Membrane Protrusion: a Possible Mechanism for Cell-to-Cell Spreading. *Infect. Immun.* 68, 5377–5384. <https://doi.org/10.1128/IAI.68.9.5377-5384.2000>.
14. Welch, M.D., and Way, M. (2013). Arp2/3-Mediated Actin-Based Motility: A Tail of Pathogen Abuse. *Cell Host Microbe* 14, 242–255. <https://doi.org/10.1016/j.chom.2013.08.011>.
15. McMahon, H.T., and Boucrot, E. (2011). Molecular mechanism and physiological functions of clathrin-mediated endocytosis. *Nat. Rev. Mol. Cell Biol.* 12, 517–533. <https://doi.org/10.1038/nrm3151>.
16. Fukumatsu, M., Ogawa, M., Arakawa, S., Suzuki, M., Nakayama, K., Shimizu, S., Kim, M., Mimuro, H., and Sasakawa, C. (2012). Shigella Targets Epithelial Tricellular Junctions and Uses a Noncanonical Clathrin-Dependent Endocytic Pathway to Spread Between Cells. *Cell Host Microbe* 11, 325–336. <https://doi.org/10.1016/j.chom.2012.03.001>.
17. Schwarz, S., Singh, P., Robertson, J.D., LeRoux, M., Skerrett, S.J., Goodlett, D.R., West, T.E., and Mougous, J.D. (2014). VgrG-5 Is a *Burkholderia* Type VI Secretion System-Exported Protein Required for Multinucleated Giant Cell Formation and Virulence. *Infect. Immun.* 82, 1445–1452. <https://doi.org/10.1128/IAI.01368-13>.
18. Dilucca, M., Ramos, S., Shkarina, K., Santos, J.C., and Broz, P. (2021). Guanylate-Binding Protein-Dependent Noncanonical Inflammasome Activation Prevents *Burkholderia thailandensis*-Induced Multinucleated Giant Cell Formation. *mBio* 12, e0205421. <https://doi.org/10.1128/mBio.02054-21>.
19. Pukatzki, S., Ma, A.T., Revel, A.T., Sturtevant, D., and Mekalanos, J.J. (2007). Type VI secretion system translocates a phage tail spike-like protein into target cells where it cross-links actin. *Proc. Natl. Acad. Sci. USA* 104, 15508–15513. <https://doi.org/10.1073/pnas.0706532104>.
20. Hood, R.D., Singh, P., Hsu, F., Güvener, T., Carl, M.A., Trinidad, R.R.S., Silverman, J.M., Ohlson, B.B., Hicks, K.G., Plemel, R.L., et al. (2010). A Type VI Secretion System of *Pseudomonas aeruginosa* Targets a Toxin to Bacteria. *Cell Host Microbe* 7, 25–37. <https://doi.org/10.1016/j.chom.2009.12.007>.
21. Ma, A.T., McAuley, S., Pukatzki, S., and Mekalanos, J.J. (2009). Translocation of a *Vibrio cholerae* Type VI Secretion Effector Requires Bacterial Endocytosis by Host Cells. *Cell Host Microbe* 5, 234–243. <https://doi.org/10.1016/j.chom.2009.02.005>.
22. Pukatzki, S., Ma, A.T., Sturtevant, D., Krastins, B., Sarracino, D., Nelson, W.C., Heidelberg, J.F., and Mekalanos, J.J. (2006). Identification of a conserved bacterial protein secretion system in *Vibrio cholerae* using the *Dictyostelium* host model system. *Proc. Natl. Acad. Sci. USA* 103, 1528–1533. <https://doi.org/10.1073/pnas.0510322103>.
23. Brunet, Y.R., Zoued, A., Boyer, F., Douzi, B., and Cascales, E. (2015). The Type VI Secretion TssEFGK-VgrG Phage-Like Baseplate Is Recruited to the TssJLM Membrane Complex via Multiple Contacts and Serves As Assembly Platform for Tail Tube/Sheath Polymerization. *PLOS Genet.* 11, e1005545. <https://doi.org/10.1371/journal.pgen.1005545>.
24. Durand, E., Nguyen, V.S., Zoued, A., Logger, L., Péhau-Arnaudet, G., Aschtgen, M.-S., Spinelli, S., Desmyter, A., Bardiaux, B., Dujeancourt, A., et al. (2015). Biogenesis and structure of a type VI secretion membrane core complex. *Nature* 523, 555–560. <https://doi.org/10.1038/nature14667>.
25. Brunet, Y.R., Zoued, A., Boyer, F., Douzi, B., and Cascales, E. (2015). The Type VI Secretion TssEFGK-VgrG Phage-Like Baseplate Is Recruited to the TssJLM Membrane Complex via Multiple Contacts and Serves As Assembly Platform for Tail Tube/Sheath Polymerization. *PLoS Genet* 11, e1005545. <https://doi.org/10.1371/journal.pgen.1005545>.
26. Szwedziak, P., and Pilhofer, M. (2019). Bidirectional contraction of a type six secretion system. *Nat. Commun.* 10, 1565. <https://doi.org/10.1038/s41467-019-09603-1>.
27. Wang, J., Brackmann, M., Castaño-Díez, D., Kudryashev, M., Goldie, K.N., Maier, T., Stahlberg, H., and Basler, M. (2017). Cryo-EM structure of the extended type VI secretion system sheath-tube complex. *Nat. Microbiol.* 2, 1507–1512. <https://doi.org/10.1038/s41564-017-0020-7>.
28. Basler, M., Pilhofer, M., Henderson, G.P., Jensen, G.J., and Mekalanos, J.J. (2012). Type VI secretion requires a dynamic contractile phage tail-like structure. *Nature* 483, 182–186. <https://doi.org/10.1038/nature10846>.
29. Cianfanelli, F.R., Monlezun, L., and Coulthurst, S.J. (2016). Aim, Load, Fire: The Type VI Secretion System, a Bacterial Nanoweapon. *Trends Microbiol.* 24, 51–62. <https://doi.org/10.1016/j.tim.2015.10.005>.
30. Wood, T.E., Howard, S.A., Wettstadt, S., and Filloux, A. (2019). PAAR proteins act as the ‘sorting hat’ of the type VI secretion system. *Microbiology (Reading)* 165, 1203–1218. <https://doi.org/10.1099/mic.0.000842>.
31. Schneider, M.M., Butch, S.A., Ho, B.T., Basler, M., Mekalanos, J.J., and Leiman, P.G. (2013). PAAR-repeat proteins sharpen and diversify the type VI secretion system spike. *Nature* 500, 350–353. <https://doi.org/10.1038/nature12453>.
32. Basler, M., and Mekalanos, J.J. (2012). Type 6 Secretion Dynamics Within and Between Bacterial Cells. *Science* 337, 815. <https://doi.org/10.1126/science.1222901>.
33. Bönemann, G., Pietrosik, A., Diemand, A., Zentgraf, H., and Mogk, A. (2009). Remodelling of VipA/VipB tubules by ClpV-mediated threading is crucial for type VI protein secretion. *EMBO J.* 28, 315–325. <https://doi.org/10.1038/embj.2008.269>.
34. Mougous, J.D., Cuff, M.E., Raunser, S., Shen, A., Zhou, M., Gifford, C.A., Goodman, A.L., Joachimiak, G., Ordoñez, C.L., Lory, S., et al. (2006). A Virulence Locus of *Pseudomonas aeruginosa* Encodes a Protein Secretion Apparatus. *Science* 312, 1526–1530. <https://doi.org/10.1126/science.1128393>.
35. Toesca, I.J., French, C.T., and Miller, J.F. (2014). The Type VI Secretion System Spike Protein VgrG5 Mediates Membrane Fusion during Intercellular Spread by Pseudomallei Group Burkholderia Species. *Infect. Immun.* 82, 1436–1444. <https://doi.org/10.1128/IAI.01367-13>.
36. Barret, M., Egan, F., Fargier, E., Morrissey, J.P., and O'gara, F. (2011). Genomic analysis of the type VI secretion systems in *Pseudomonas* spp.: novel clusters and putative effectors uncovered. *Microbiology (Reading)* 157, 1726–1739. <https://doi.org/10.1099/mic.0.048645-0>.
37. Ho, B.T., Dong, T.G., and Mekalanos, J.J. (2014). A View to a Kill: The Bacterial Type VI Secretion System. *Cell Host Microbe* 15, 9–21. <https://doi.org/10.1016/j.chom.2013.11.008>.
38. Russell, A.B., LeRoux, M., Hathazi, K., Agnello, D.M., Ishikawa, T., Wiggins, P.A., Wai, S.N., and Mougous, J.D. (2013). Diverse type VI secretion phospholipases are functionally plastic antibacterial effectors. *Nature* 496, 508–512. <https://doi.org/10.1038/nature12074>.

39. Whitney, J.C., Beck, C.M., Goo, Y.A., Russell, A.B., Harding, B.N., De Leon, J.A., Cunningham, D.A., Tran, B.Q., Low, D.A., Goodlett, D.R., et al. (2014). Genetically distinct pathways guide effector export through the type VI secretion system: Effector export pathways of type VI secretion. *Mol. Microbiol.* 92, 529–542. <https://doi.org/10.1111/mmi.12571>.
40. Hopf, V., Göhler, A., Eske-Pogodda, K., Bast, A., Steinmetz, I., and Breitbach, K. (2014). BPSS1504, a Cluster 1 Type VI Secretion Gene, Is Involved in Intracellular Survival and Virulence of *Burkholderia pseudomallei*. *Infect. Immun.* 82, 2006–2015. <https://doi.org/10.1128/IAI.01544-14>.
41. Lennings, J., West, T.E., and Schwarz, S. (2019). The *Burkholderia* Type VI Secretion System 5: Composition, Regulation and Role in Virulence. *Front. Microbiol.* 9, 3339. <https://doi.org/10.3389/fmicb.2018.03339>.
42. Kostow, N., and Welch, M.D. (2022). Plasma membrane protrusions mediate host cell-cell fusion induced by *Burkholderia thailandensis*. *Mol. Biol. Cell* 33, ar70. <https://doi.org/10.1091/mbc.E22-02-0056>.
43. Saiprom, N., Sangsri, T., Tandhavanant, S., Sengyee, S., Phunpang, R., Preechanukul, A., Surin, U., Tuanyok, A., Lertmemongkolchai, G., Chantratita, W., et al. (2020). Genomic loss in environmental and isogenic morphotype isolates of *Burkholderia pseudomallei* is associated with intracellular survival and plaque-forming efficiency. *PLoS Negl. Trop. Dis.* 14, e0008590. <https://doi.org/10.1371/journal.pntd.0008590>.
44. Harley, V.S., Dance, D.A., Drasar, B.S., and Tovey, G. (1998). Effects of *Burkholderia pseudomallei* and other *Burkholderia* species on eukaryotic cells in tissue culture. *Microbios* 96, 71–93.
45. Burtnick, M.N., DeShazer, D., Nair, V., Gherardini, F.C., and Brett, P.J. (2010). *Burkholderia mallei* Cluster 1 Type VI Secretion Mutants Exhibit Growth and Actin Polymerization Defects in RAW 264.7 Murine Macrophages. *Infect. Immun.* 78, 88–99. <https://doi.org/10.1128/IAI.00985-09>.
46. Shalom, G., Shaw, J.G., and Thomas, M.S. (2007). In vivo expression technology identifies a type VI secretion system locus in *Burkholderia pseudomallei* that is induced upon invasion of macrophages. *Microbiology (Reading)* 153, 2689–2699. <https://doi.org/10.1099/mic.0.2007/006585-0>.
47. Kespichayawattana, W., Intachote, P., Utaisincharoen, P., and Sirisinha, S. (2004). Virulent *Burkholderia pseudomallei* is more efficient than avirulent *Burkholderia thailandensis* in invasion of and adherence to cultured human epithelial cells. *Microb. Pathog.* 36, 287–292. <https://doi.org/10.1016/j.micpath.2004.01.001>.
48. Lum, M., Attridge, S.R., and Morona, R. (2013). Impact of Dynasore an Inhibitor of Dynamin II on *Shigella flexneri* Infection. *PLoS ONE* 8, e84975. <https://doi.org/10.1371/journal.pone.0084975>.
49. Macia, E., Ehrlich, M., Massol, R., Boucrot, E., Brunner, C., and Kirchhausen, T. (2006). Dynasore, a Cell-Permeable Inhibitor of Dynamin. *Dev. Cell* 10, 839–850. <https://doi.org/10.1016/j.devcel.2006.04.002>.
50. Park, R.J., Shen, H., Liu, L., Liu, X., Ferguson, S.M., and De Camilli, P. (2013). Dynamin triple knockout cells reveal off target effects of commonly used dynamin inhibitors. *J. Cell Sci.* 126, 5305–5312. <https://doi.org/10.1242/jcs.138578>.
51. Hughes, R.C. (1999). Secretion of the galectin family of mammalian carbohydrate-binding proteins. *Biochim. Biophys. Acta* 1473, 172–185. [https://doi.org/10.1016/S0304-4165\(99\)00177-4](https://doi.org/10.1016/S0304-4165(99)00177-4).
52. Jia, J., Claude-Taupin, A., Gu, Y., Choi, S.W., Peters, R., Bissa, B., Mudd, M.H., Allers, L., Pallikkuth, S., Lidke, K.A., et al. (2020). Galectin-3 Coordinates a Cellular System for Lysosomal Repair and Removal. *Dev. Cell* 52, 69–87.e8. <https://doi.org/10.1016/j.devcel.2019.10.025>.
53. Paz, I., Sachse, M., Dupont, N., Mounier, J., Cederfur, C., Enninga, J., Leffler, H., Poirier, F., Prevost, M.-C., Lafont, F., and Sansonetti, P. (2010). Galectin-3, a marker for vacuole lysis by invasive pathogens. *Cell. Microbiol.* 12, 530–544. <https://doi.org/10.1111/j.1462-5822.2009.01415.x>.
54. Sangsri, T., Saiprom, N., Tubsuwan, A., Monk, P., Partridge, L.J., and Chantratita, N. (2020). Tetraspanins are involved in *Burkholderia pseudomallei*-induced cell-to-cell fusion of phagocytic and non-phagocytic cells. *Sci. Rep.* 10, 17972. <https://doi.org/10.1038/s41598-020-74737-y>.
55. Whiteley, L., Haug, M., Klein, K., Willmann, M., Bohn, E., Chiantia, S., and Schwarz, S. (2017). Cholesterol and host cell surface proteins contribute to cell-cell fusion induced by the *Burkholderia* type VI secretion system 5. *PLoS ONE* 12, e0185715. <https://doi.org/10.1371/journal.pone.0185715>.
56. Basler, M., Ho, B.T., and Mekalanos, J.J. (2013). Tit-for-Tat: Type VI Secretion System Counterattack during Bacterial Cell-Cell Interactions. *Cell* 152, 884–894. <https://doi.org/10.1016/j.cell.2013.01.042>.
57. Ho, B.T., Basler, M., and Mekalanos, J.J. (2013). Type 6 Secretion System-Mediated Immunity to Type 4 Secretion System-Mediated Gene Transfer. *Science* 342, 250–253. <https://doi.org/10.1126/science.1243745>.
58. Wilton, M., Wong, M.J.Q., Tang, L., Liang, X., Moore, R., Parkins, M.D., Lewenza, S., and Dong, T.G. (2016). Chelation of Membrane-Bound Cations by Extracellular DNA Activates the Type VI Secretion System in *Pseudomonas aeruginosa*. *Infect. Immun.* 84, 2355–2361. <https://doi.org/10.1128/IAI.00233-16>.
59. Lin, L., Capozzoli, R., Ferrand, A., Plum, M., Vettiger, A., and Basler, M. (2022). Subcellular localization of Type VI secretion system assembly in response to cell-cell contact. *EMBO J.* 41, e108595. <https://doi.org/10.1525/embj.2021108595>.
60. Stockton, J.L., and Torres, A.G. (2020). Multinucleated Giant Cell Formation as a Portal to Chronic Bacterial Infections. *Microorganisms* 8, 1637. <https://doi.org/10.3390/microorganisms8111637>.
61. Wong, K.T., Puthucheary, S.D., and Vadivelu, J. (1995). The histopathology of human melioidosis. *Histopathology* 26, 51–55. <https://doi.org/10.1111/j.1365-2559.1995.tb00620.x>.
62. Chow, T.K., Eu, L.C., Chin, K.F., Ong, K.C., Palloor, J., Vadivelu, J., and Wong, K.T. (2016). Incidental Splenic Granuloma Due to *Burkholderia pseudomallei*: A Case of Asymptomatic Latent Melioidosis? *Am. J. Trop. Med. Hyg.* 94, 522–524. <https://doi.org/10.4269/ajtmh.15-0774>.
63. Amemiya, K., Dankmeyer, J.L., Bearss, J.J., Zeng, X., Stonier, S.W., Soffler, C., Cote, C.K., Welkos, S.L., Fetterer, D.P., Chance, T.B., et al. (2020). Dysregulation of TNF- α and IFN- γ expression is a common host immune response in a chronically infected mouse model of melioidosis when comparing multiple human strains of *Burkholderia pseudomallei*. *BMC Immunol.* 21, 5. <https://doi.org/10.1186/s12865-020-0333-9>.
64. Ku, J.W.K., Chen, Y., Lim, B.J.W., Gasser, S., Crasta, K.C., and Gan, Y.-H. (2020). Bacterial-induced cell fusion is a danger signal triggering cGAS-STING pathway via micronuclei formation. *Proc. Natl. Acad. Sci. USA* 117, 15923–15934. <https://doi.org/10.1073/pnas.2006908117>.
65. Roux, A., Koster, G., Lenz, M., Sorre, B., Manneville, J.-B., Nassoy, P., and Bassereau, P. (2010). Membrane curvature controls dynamin polymerization. *Proc. Natl. Acad. Sci. USA* 107, 4141–4146. <https://doi.org/10.1073/pnas.0913734107>.
66. Liu, Y.-W., Neumann, S., Ramachandran, R., Ferguson, S.M., Pucadyil, T.J., and Schmid, S.L. (2011). Differential curvature sensing and generating activities of dynamin isoforms provide opportunities for tissue-specific regulation. *Proc. Natl. Acad. Sci. USA* 108, E234–E242. <https://doi.org/10.1073/pnas.1102710108>.
67. Cook, T., Mesa, K., and Urrutia, R. (1996). Three Dynamin-Encoding Genes Are Differentially Expressed in Developing Rat Brain. *J. Neurochem.* 67, 927–931. <https://doi.org/10.1046/j.1471-4159.1996.67030927.x>.
68. Cao, H., Garcia, F., and McNiven, M.A. (1998). Differential Distribution of Dynamin Isoforms in Mammalian Cells. *Mol. Biol. Cell* 9, 2595–2609. <https://doi.org/10.1091/mbc.9.9.2595>.
69. Daussy, C.F., and Wodrich, H. (2020). “Repair Me if You Can”: Membrane Damage, Response, and Control from the Viral Perspective. *Cells* 9, 2042. <https://doi.org/10.3390/cells9092042>.
70. Skowrya, M.L., Schlesinger, P.H., Naismith, T.V., and Hanson, P.I. (2018). Triggered recruitment of ESCRT machinery promotes endolysosomal repair. *Science* 360, eaar5078. <https://doi.org/10.1126/science.aar5078>.

71. Boyle, K.B., and Randow, F. (2013). The role of 'eat-me' signals and autophagy cargo receptors in innate immunity. *Curr. Opin. Microbiol.* 16, 339–348. <https://doi.org/10.1016/j.mib.2013.03.010>.
72. Gong, L., Cullinan, M., Treerat, P., Ramm, G., Prescott, M., Adler, B., Boyce, J.D., and Devenish, R.J. (2011). The *Burkholderia pseudomallei* Type III Secretion System and BopA Are Required for Evasion of LC3-Associated Phagocytosis. *PLoS ONE* 6, e17852. <https://doi.org/10.1371/journal.pone.0017852>.
73. Baum, L.G., Garner, O.B., Schaefer, K., and Lee, B. (2014). Microbe-Host Interactions are Positively and Negatively Regulated by Galectin-Glycan Interactions. *Front. Immunol.* 5, 284. <https://doi.org/10.3389/fimmu.2014.00284>.
74. Baquero, E., Albertini, A.A., Vachette, P., Lepault, J., Bressanelli, S., and Gaudin, Y. (2013). Intermediate conformations during viral fusion glycoprotein structural transition. *Curr. Opin. Virol.* 3, 143–150. <https://doi.org/10.1016/j.coviro.2013.03.006>.
75. Klein, D.E., Choi, J.L., and Harrison, S.C. (2013). Structure of a Dengue Virus Envelope Protein Late-Stage Fusion Intermediate. *J. Virol.* 87, 2287–2293. <https://doi.org/10.1128/JVI.02957-12>.
76. Vance, T.D.R., and Lee, J.E. (2020). Virus and eukaryote fusogen superfamilies. *Curr. Biol.* 30, R750–R754. <https://doi.org/10.1016/j.cub.2020.05.029>.
77. Campbell-Valois, F.-X., Schnupf, P., Nigro, G., Sachse, M., Sansonetti, P.J., and Parsot, C. (2014). A Fluorescent Reporter Reveals On/Off Regulation of the *Shigella* Type III Secretion Apparatus during Entry and Cell-to-Cell Spread. *Cell Host Microbe* 15, 177–189. <https://doi.org/10.1016/j.chom.2014.01.005>.
78. Duncan-Lowey, J.K., Wiscovitch, A.L., Wood, T.E., Goldberg, M.B., and Russo, B.C. (2020). *Shigella flexneri* Disruption of Cellular Tension Promotes Intercellular Spread. *Cell Rep.* 33, 108409. <https://doi.org/10.1016/j.celrep.2020.108409>.
79. Köster, S., van Pee, K., Hudel, M., Leustik, M., Rhinow, D., Kühlbrandt, W., Chakraborty, T., and Yıldız, Ö. (2014). Crystal structure of listeriolysin O reveals molecular details of oligomerization and pore formation. *Nat. Commun.* 5, 3690. <https://doi.org/10.1038/ncomms4690>.
80. Page, A.-L., Ohayon, H., Sansonetti, P.J., and Parsot, C. (1999). The secreted IpaB and IpaC invasins and their cytoplasmic chaperone IpgC are required for intercellular dissemination of *Shigella flexneri*. *Cell. Microbiol.* 1, 183–193. <https://doi.org/10.1046/j.1462-5822.1999.00019.x>.
81. Ruan, Y., Rezelj, S., Bedina Zavec, A., Anderluh, G., and Scheuring, S. (2016). Listeriolysin O Membrane Damaging Activity Involves Arc Formation and Lineaction – Implication for *Listeria monocytogenes* Escape from Phagocytic Vacuole. *PLoS Pathog.* 12, e1005597. <https://doi.org/10.1371/journal.ppat.1005597>.
82. Kasper, C.A., Sorg, I., Schmutz, C., Tschan, T., Wischnewski, H., Kim, M.L., and Arriumerou, C. (2010). Cell-cell propagation of NF-κB transcription factor and MAP kinase activation amplifies innate immunity against bacterial infection. *Immunity* 33, 804–816. <https://doi.org/10.1016/j.immuni.2010.10.015>.
83. Fazli, M., Harrison, J.J., Gambino, M., Givskov, M., and Tolker-Nielsen, T. (2015). In-Frame and Unmarked Gene Deletions in *Burkholderia cenocepacia* via an Allelic Exchange System Compatible with Gateway Technology. *Appl. Environ. Microbiol.* 81, 3623–3630. <https://doi.org/10.1128/AEM.03909-14>.
84. Doyon, J.B., Zeitler, B., Cheng, J., Cheng, A.T., Cherone, J.M., Santiago, Y., Lee, A.H., Vo, T.D., Doyon, Y., Miller, J.C., et al. (2011). Rapid and efficient clathrin-mediated endocytosis revealed in genome-edited mammalian cells. *Nat. Cell Biol.* 13, 331–337. <https://doi.org/10.1038/ncb2175>.
85. Cutler, K.J., Stringer, C., Lo, T.W., Rappez, L., Stroustrup, N., Brook Peterson, S., Wiggins, P.A., and Mougous, J.D. (2022). Omnipose: a high-precision morphology-independent solution for bacterial cell segmentation. *Nat. Methods* 19, 1438–1448. <https://doi.org/10.1038/s41592-022-01639-4>.
86. Schindelin, J., Arganda-Carreras, I., Frise, E., Kaynig, V., Longair, M., Pietzsch, T., Preibisch, S., Rueden, C., Saalfeld, S., Schmid, B., et al. (2012). Fiji: an open-source platform for biological-image analysis. *Nat. Methods* 9, 676–682. <https://doi.org/10.1038/nmeth.2019>.
87. Schneider, C.A., Rasband, W.S., and Eliceiri, K.W. (2012). NIH Image to ImageJ: 25 years of image analysis. *Nat. Methods* 9, 671–675. <https://doi.org/10.1038/nmeth.2089>.

STAR★METHODS

KEY RESOURCES TABLE

REAGENT or RESOURCE	SOURCE	IDENTIFIER
Antibodies		
LC3B Antibody Kit for Autophagy	ThermoFisher Scientific	Cat# L10382
Goat anti-Rabbit IgG (H+L) Highly Cross-Adsorbed Secondary Antibody, Alexa Fluor™ Plus 647	Invitrogen™	A32733; RRID:AB_2866492
Recombinant anti-LAMP1 antibody	Abcam	Ab289548
Goat anti-mouse IgG H&L (Alexa Fluor ® 647)	Abcam	Ab150115; RRID:AB_2687948
Bacterial and virus strains		
<i>Burkholderia thailandensis</i> E264 wild-type	Ku et al. ⁶⁴	N/A
<i>Burkholderia thailandensis</i> E264 Δhcp-5	This study	N/A
<i>Burkholderia thailandensis</i> E264 ΔvgrG-5	Ku et al. ⁶⁴	N/A
<i>Burkholderia thailandensis</i> tssB-5-mScarlet-I	This study	N/A
<i>Burkholderia thailandensis</i> tssB-5-mNeonGreen	This study	N/A
<i>Burkholderia thailandensis</i> tssB-5-mCherry2	This study	N/A
<i>Burkholderia thailandensis</i> tssB-5-msfGFP	This study	N/A
<i>Burkholderia thailandensis</i> ΔvgrG-5, tssB-5-mScarletI	This study	N/A
<i>Burkholderia thailandensis</i> Δhcp-5, tssB-5-mScarletI	This study	N/A
<i>Burkholderia thailandensis</i> BTH_I_TN7L::pCS12-mCherry2	This study	N/A
<i>Burkholderia thailandensis</i> BTH_I_TN7L::pCS12-mCherry2, Δhcp-5	This study	N/A
<i>Burkholderia thailandensis</i> BTH_I_TN7L::pCS12-mCherry2, ΔvgrG-5	This study	N/A
<i>Burkholderia thailandensis</i> tssB-5-mCherry2, ΔtagD-5	This study	N/A
<i>Burkholderia thailandensis</i> ΔtagB-5, tssB-5-mNeonGreen	This study	N/A
<i>Burkholderia thailandensis</i> ΔtagC-5, tssB-5-mCherry2	This study	N/A
<i>Burkholderia thailandensis</i> ΔtagAB-5, tssB-5-mCherry2	This study	N/A
<i>Shigella flexneri</i> M90t pMW211-dsRed	Kasper et al. ⁸²	N/A
Chemicals, peptides, and recombinant proteins		
DMEM high glucose	Sigma-Aldrich Chemie GmbH	Cat# D5796
Ham's F-12 Nutrient Mix, GlutaMAX™ Supplement	ThermoFisher Scientific	Cat# 31765035
Gibco™ Opti-MEM™ I Reduced Serum Medium, no phenol red	Fisher Scientific	Cat #11520386
Foetal Calf Serum (FCS), Heat Inactivated	BioConcept Ltd.	Cat# 2-01F16-I
Bovine Serum Albumin	Sigma-Aldrich	Cat# A9647
4-Chloro-DL-phenylalanine, 98+%	Chemie Brunschwig AG	Cat# ALFA1323-18
Neutral Red	Fluka Chemie GmbH	Cat# 77210
Dynasore hydrate	Sigma-Aldrich	Cat# D7693

(Continued on next page)

Continued

REAGENT or RESOURCE	SOURCE	IDENTIFIER
Dimethyl sulfoxide	Sigma-Aldrich	Cat# 41639
4-Hydroxytamoxifen	Sigma-Aldrich	Cat# H6278
Hoechst 33342 Solution (20mM)	ThermoFisher	Cat# 62249
CellMask™ Plasma Membrane Stains	ThermoFisher	Cat# C10046
M9, Minimal Salts, 5X	Sigma-Aldrich	Cat# M6030
Experimental models: Cell lines		
Human: HeLa-CCL-2 cells	ATCC	Cat# CCL-2™ Lot# 58469359; RRID:CVCL_0030
Human: HeLa-CCL-2, Galectin-3-GFP cells	Provided by Prof Christoph Dehio (University of Basel)	N/A
Human: HeLa-CCL-2, Galectin-3-mApple cells	Provided by Prof Christoph Dehio (University of Basel)	N/A
Human: A549 cells	ATCC	Cat# 86012804 Lot# 18F020
Human: SK-MEL-2 cell, DNM2-GFP	Provided by Prof Aurélien Roux (University of Geneva)	N/A
Mouse: Fibroblasts, dynamin conditional knock-out	Provided by Prof Pietro De Camilli (Yale University)	N/A
Oligonucleotides		
TCAGTATCTAGACGCGAACGCGTTCC	This study	tssB-5_F1_XbaI.FOR
CTGTACAAGCTGGGCC	This study	tssB-5-mCherry2_F1.REV
TCGACGAACAATG		
AGGCCAGCTTGACAGCTCGTCC	This study	tssB-5-mCherry2_F2.FOR
GCCTCGACGAAACAGCGGCCGAGGAG	This study	tssB-5_F2.REV
CCTGCGGCCGTTCTCGAGGC	This study	tssB-5_F3.FOR
TCAGTAAGCTTGTCTCAGAGGTCGGC	This study	tssB-5_F3_HindIII.REV
CTGTACAAACTGGGCCTCGACG	This study	tssB-5-mNeonGreen_F1.REV
AGGCCAGTTGTACAGCTATCCATAC	This study	tssB-5-mNeonGreen_F2.FOR
CTGTATAAACTGGGCCTCGACG	This study	tssB-5-mScarlet-I_F1.REV
CGAGGCCAGTTATACAGTTATCCAT ACCACC	This study	tssB-5-mScarlet-I_F2.FOR
CTCTACAAACTGGGCCTCGACGAA AATG	This study	tssB-5-msfGFP_F1.REV
AGGCCAGTTGTAGAGCTC	This study	tssB-msfGFP_F2.FOR
CATCGCCTCGTACGCATAG	This study	tssB-5_Det.FOR
CATCCGGATCGTTCATC	This study	tssB-5_Det.REV
TCAGTAGGGCCCTCAGCCGAGATCGAT GCGCTC	This study	TN7L_PC12-TagC-5.For
AGTCATGGTACCAAGCTGTTGACTCGC TTGGGATTTCGGAATATCATGCCGG TCTGACAATCGGATCGAGCTCGAAAG GACAAGCATATGGACCGCGCCCGAAC	This study	TN7L_PC12-TagC-5.Rev
TCAGTAGGGCCCTTAACTCATCACCA TCACTTCTGCTG	This study	TN7L_PC12-TagD-5.For
AGTCATGGTACCAAGCTGTTGACTCGC TTGGGATTTCGGAATATCATGCCGG TCTGACAATCGGATCGAGCTCGAAAG GACAAGCATATGGACCGCGCCCGAAC	This study	TN7L_PC12-TagD-5.Rev
TCAGTAGGGCCCTCATCGTTGGCG CGGTC	This study	TN7L_PC12-TagB-5.For

(Continued on next page)

Continued

REAGENT or RESOURCE	SOURCE	IDENTIFIER
AGTCATGGTACCGAGCTGTTGACTCGC TTGGGATTTCGGAATATCATGCCGG GTCTGACAATCGGATCGAGCTTCGAA AGGACAAGCATATGTCGACACAGTT CACGCG	This study	TN7L_PC12-TagB-5.Rev
TCAGTAGGGCCCTCAGCGGGATGAC GCGAGTTC	This study	TN7L_PC12-TagAB-5.For
AGTCATGGTACCGAGCTGTTGACTCGC TTGGGATTTCGGAATATCATGCCGG GTCTGACAATCGGATCGAGCTTCGAA AGGACAAGCATATGAAAATCGTCAA CCCGAGTCG	This study	TN7L_PC12-TagAB-5.Rev
TCAGTAGGGCCCTTACTTGACAGCT CGTCCATGCC	This study	TN7L_PC12-mCherry2.FOR
AGTCATGGTACCGAGCTGTTGACTCGC TTGGGATTTCGGAATATCATGCCGG GTCTGACAATCGGATCGAGCTTCGAA AGGACAAGCATATGGTGAGCAAGGGC GAGGAGGATAAC	This study	TN7L_PC12-mCherry2.REV
GTCGGTGACGGTGGAGTAG	This study	BTH_II_TN7_Det.FOR
TGTGAATGGTCAGACGCTGTTGC	This study	BTH_II_TN7_Det.Rev
GCGTTCGTCGTCCACTGGGA	This study	BTH_I_TN7_Det.FOR
CCGTGACGGTGGAGATAAG	This study	BTH_I_TN7_Det.Rev
Recombinant DNA		
pDONRPEX18Tp-Scel-pheS	Addgene	Plasmid#11608; RRID:Addgene_111608
pUC18T-mini-Tn7T-Tp	Addgene	Plasmid#65024; RRID:Addgene_65024
pTNS2	Addgene	Plasmid#64968; RRID:Addgene_64968
pEGFP-C1 Lifeact-EGFP	Dilucca et al. ¹⁸	N/A
pDONRPEX18Tp-TssB-5-mScarlet-I	This study	N/A
pDONRPEX18Tp-TssB-5-mCherry2	This study	N/A
pDONRPEX18Tp-TssB-5-msfGFP	This study	N/A
pDONRPEX18Tp-TssB-5-mNeonGreen	This study	N/A
pDONRPEX18Tp-ΔTagB-5	This study	N/A
pDONRPEX18Tp-ΔTagC-5	This study	N/A
pDONRPEX18Tp-ΔTagAB-5	This study	N/A
pDONRPEX18Tp-ΔTagD-5	This study	N/A
pUC18T-PC12-mCherry2	This study	N/A
Software and algorithms		
GraphPad Prism 9	N/A	http://www.graphpad.com
Fiji ImageJ	National Institute of Health	https://imagej.net/
FlowJo	FlowJo LLC	RRID: SCR_008520

RESOURCE AVAILABILITY

Lead contact

Further information and requests for resources should be directed to the lead contact, Marek Basler (marek.basler@unibas.ch)

Materials availability

This study did not generate new unique materials

Data and code availability

- All data reported in this paper will be shared by the [lead contact](#) upon request.
- This work did not use or generate new codes.
- Any additional information required to reanalyze the data reported in this paper is available from the [lead contact](#) upon request.

EXPERIMENTAL MODEL AND STUDY PARTICIPANT DETAILS

Bacterial strains, plasmids, and culturing conditions

Bacterial strains used in this study are listed in the [key resource table](#). Bacterial strains were grown in LB media overnight at 37°C with aeration. When appropriate, antibiotics were added at the following concentrations: 50 µg/mL of trimethoprim for *E. coli* and 200 µg/mL for *B. thailandensis*; 30 µg/mL of gentamicin for *E. coli*. Mutant strains were generated by allelic exchange using the vector pDONRPEX-18Tp-Scel-pheS.⁸³ The vector was cut with Apal and KpnI or HindIII and XbaI. In short, pDONRPEX-18Tp-Scel-pheS derivatives were conjugated into *B. thailandensis* strains by *E. coli* SM10 λpir. The conjugants were selected by trimethoprim resistance. Counter selection were performed on M9 minimal medium agar plates with 0.4% glucose and 0.1% (w/v) 4-chlorophenylalanine.

We constructed in-frame deletions by fusing codons encoding the first five amino acid residues to the codons encoding the last five amino acid residues of the gene of interest. Homologous arms were at least 1000 bp upstream and downstream of the gene of interest. The fragments were PCR amplified and cloned into pDONRPEX-18Tp-Scel-pheS via Gibson assembly (NEB) or restriction digest and ligation and sequenced. For constructing sheath protein TssB-5 fusion with fluorophores, a linker with 6 amino acids (AAAGGG) were added between the TssB-5 and fluorophore codons. For constitutive expression of proteins, we used the plasmid pUC18T-mini-Tn7-Tp to insert the fragments at the *attN7* site near the *glmS* locus.

Mammalian cell lines and culturing

The cell lines HeLa cells (CCL-2, ATCC), A549 lung cells (CCL-185, ATCC), SK-MEL-2 cells (HTB-68, ATCC), and mouse fibroblasts (generated by the De Camilli lab, Yale School of Medicine) were used in this study.⁵⁰ The HeLa and SK-MEL-2 cells were cultured at 37°C with 5% CO₂ with DMEM (Sigma-Aldrich) supplemented with 10% heat-inactivated fetal calf serum (FCS, BioConcept AG), and A549 lung cells with Ham's F-12 media (Sigma-Aldrich) supplemented with 10% heat-inactivated FCS. SK-MEL-2 cells expressing DNM2-GFP were provided by A. Roux.⁸⁴ Wild-type mouse fibroblasts were cultured in DMEM supplemented with 10% heat-inactivated FCS. Dynamin knock out cells were induced by 4-hydroxytamoxifen from wild-type mouse fibroblasts. To induce dynamin knock out, 2 µM of 4-hydroxytamoxifen into the DMEM medium for 48 hours. Then, cells were split and 300 nM of 4-hydroxytamoxifen was added for 72 hours.⁵⁰ All experiments were performed using cells from passages 2 to 10. All cell lines used in this study were tested negative for mycoplasma contamination by MycoStrip (InvivoGen).

METHOD DETAILS

Infection assays

A549, SK-MEL-2 and HeLa cells were seeded at 8 × 10⁴ cells per well, mouse fibroblasts were seeded at 6 × 10⁴ cells per well on µ-slide 8 well glass bottom (Ibidi GmbH) 24 hours prior to infection. Bacterial strains were grown in low salt LB overnight at 37°C with aeration. The bacterial cells were then subcultured in a 1:100 dilution and grown until mid-log phase in low salt LB. Bacterial cells and mammalian cells were washed in Opti-MEM™ Reduced Serum Medium with GlutaMAX™ supplement (Sigma-Aldrich). The bacterial cells were then added to the mammalian cells at a MOI of 50 or 100 unless otherwise specified and the µ-slide 8 well glass bottom slides were spun down at 300 × g for 5 min. After 1 hour post-infection, Opti-MEM™ supplemented with 300 µg/mL of kanamycin was added to kill extracellular bacteria. CellMask DeepRed and/or Hoechst 33342 were used to stain the infected cells at the time of imaging, as specified in the figure legends.

Flow cytometry

On the day prior to infection, 2 × 10⁶ A549 cells were seeded in a 75 cm² flask. The infection was performed as described above. At 12 hpi the cells were stained with Hoechst 3342 (1:5000 in Opti-MEM™) for 10 min. Then, the cells were washed twice with Opti-MEM™ supplemented with 300 µg/mL of kanamycin. In order to detach the cells, 0.05% Trypsin was added per flask for 5–10 min. F-12 media (Sigma-Aldrich) supplemented with 10% heat-inactivated FCS was added to the suspension. The cells were then transferred into a falcon tube, and fixed by adding 4% PFA for 10 min at RT. After fixation, the cells were centrifuged at 300 × g for 5 min and the supernatant was discarded. The pellet was re-suspended in 2% BSA to generate a single cell suspension. Prior to FACS analysis, the cells were filtered through a 35 µm mesh to exclude MNGCs. Cell analysis and sorting was conducted using a BD FACS Aria Fusion. A total of 300'000 events were analysed per condition.

Transfection

Transfection was performed based on the manufacturer protocol of FuGENE® HD Transfection Reagent (Promega). In summary, A549 lung cells were seeded 1.5 × 10⁵ cells per well on µ-slide 8 well glass bottom (Ibidi GmbH) 24 hours prior to transfection. pEGFP-C1 Lifeact-EGFP was incubated with FuGENE® HD Transfection Reagent (Promega) and the mixture was added to the A549 lung cells seeded. The cells were then incubated for 24 hours and then were infected and imaged with live-cell microscopy.

Giemsa stain and MNGC formation

To test for our strain's ability to form MNGC, we conducted a fusion assay of HeLa cells either expressing a red (galectin-3-mApple) or green (galectin-3-GFP) cytosolic fluorescent protein. We infected a mixture of the red and green HeLa cells mentioned above and

looked for formation of cells with both fluorescently labeled proteins after 12 hpi. To quantify the ability of the *B. thailandensis* strains to form MNGCs, A549 cells or mouse fibroblasts were infected as described and fixed with methanol at 15–16 hpi. Mouse fibroblasts were seeded at a lower density of 4×10^4 cells per well. They were washed with sterile water twice before staining with Giemsa stain solution (Carl Roth) for 30 minutes. After staining, the cells were washed twice with water and imaged with Olympus SpinSR bright-field 30x silicone oil objective. Fields of view were randomly taken for each bacterial strain. Fields of view without bacteria were discarded and 12 fields of view were used for analysing MNGC formation. The total number of nuclei and the number of nuclei located inside a MNGC were counted for each field of view. At least 1000 nuclei were counted for each bacterial strain. MNGC formation efficiency (expressed as percentages) was determined as: (the number of nuclei within MNGC / total number of nuclei in the field of view) × 100.

Plaque assay

A549 and mouse fibroblasts were seeded at 6×10^5 cells per well on 6-well slides. A549 cells were infected with MOI of 2 for 1 h, and mouse fibroblasts were infected with MOI of 0.2 for 1 h. The infected cell monolayers were then washed once with Opti-MEM™ supplemented with 300 µg/mL of kanamycin, and overlaid with Opti-MEM™ supplemented with 300 µg/mL of kanamycin and 0.5% agar for 22 hours. At 23 hpi, another layer of Opti-MEM™ supplemented with 300 µg/mL of kanamycin, 0.5% agar, and 0.01% neutral red was added. Plaques were observed and imaged at 31 hpi.

Counting of galectin-3 accumulations

For the quantification of galectin-3 foci during infections, HeLa galectin-3-GFP expressing cells were infected as described. *B. thailandensis* infections were performed with an MOI of 100 and *S. flexneri* infections with an MOI of 10. Images were taken between 12:30 to 16 hpi. At least 106 fields of view ($295 \times 295 \mu\text{m}$) were acquired. On these images at least 22'286 bacteria were counted with Omnipose.⁸⁵ Galectin-3 accumulations were detected with Fiji/ImageJ with “Find Maxima” (prominence = 1800) and “Analyze Particles”. To subtract background galectin-3-GFP accumulations, images of uninfected cells were similarly processed and the resulting average galectin-3-GFP background was subtracted from the results. After this the results were adjusted for galectin-3-GFP accumulations per 1000 bacteria. At least four biological replicates were analysed.

Immunofluorescence

Cells were infected as described above, and one well of cells were treated with 100 µM chloroquine as a positive control. At 17 hpi, cells were fixed and permeabilization with ice cold 100% methanol for 15 minutes. The fixed cells were washed twice with PBS. LC3B rabbit polyclonal antibody (ThermoFisher Scientific) was diluted to 0.5 µg/mL and LAMP1 mouse monoclonal antibody (Abcam) was diluted to 1 µg/mL in 1% Bovine Serum Albumin (BSA, Sigma-Aldrich) and added to the fixed cells to incubate at room temperature for 2 hours. Cells were then washed twice with PBS. Anti-rabbit (Invitrogen) and anti-mouse (Abcam) secondary antibodies were diluted 1:300 in 1% BSA and incubated with the cells overnight at 4 degrees. Cells were then washed twice with PBS and imaged.

Live-cell confocal microscopy

For live-cell imaging of infection assays, mammalian cells were stained with CellMask™ DeepRed plasma membrane stain (Thermo Fisher Scientific) at 1:10'000 dilution for 5 minutes. They were washed twice with Opti-MEM™ supplemented with 300 µg/mL of kanamycin. The confocal images were obtained with the 60x oil objective of Olympus SpinSR (CSU-W1) spinning disk confocal system, the DeltaVision OMX Flex with the EDGE confocal line scanning module or the Nikon ECLIPSE Ti2 with the Crest optics X-Light V3 spinning disk confocal system at 37°C with 5% CO₂ incubation.

QUANTIFICATION AND STATISTICAL ANALYSIS

Images were acquired from at least three biological replicates, the counted fields of view are stated in the figure legends or the main text. The images were analysed with ImageJ/Fiji.^{86,87} When quantifying T6SS-5 assemblies, the occasional non-dynamic T6SS-5 foci were not counted. GraphPad Prism 9.1.0. were used for data analysis. Two-tailed *t*-test was performed when comparing two means and one-way ANOVA with Tukey's multiple comparison test was performed when comparing multiple means. Statistical significance was defined at P<0.05 and the specific statistical testing for each experiment is listed in the figure legends.